

2010

A study of hough transform for weld extraction

Rakesh Gunaseelan

Louisiana State University and Agricultural and Mechanical College

Follow this and additional works at: https://digitalcommons.lsu.edu/gradschool_theses



Part of the [Construction Engineering and Management Commons](#)

Recommended Citation

Gunaseelan, Rakesh, "A study of hough transform for weld extraction" (2010). *LSU Master's Theses*. 2167.
https://digitalcommons.lsu.edu/gradschool_theses/2167

This Thesis is brought to you for free and open access by the Graduate School at LSU Digital Commons. It has been accepted for inclusion in LSU Master's Theses by an authorized graduate school editor of LSU Digital Commons. For more information, please contact gradetd@lsu.edu.

A STUDY OF HOUGH TRANSFORM FOR WELD EXTRACTION

A Thesis

Submitted to the Graduate Faculty of the
Louisiana State University and
Agricultural and Mechanical College
in partial fulfillment of the
requirements for the degree of
Master of Science in Industrial Engineering

in

The Department of Construction Management and Industrial
Engineering

by

Rakesh Gunaseelan

B. Tech., Dr B R Ambedkar National Institute of Technology, India,
2005

August, 2010

Acknowledgements

I sincerely thank my parents and my sister. Without their encouragement, I would not have embarked my journey to this country.

I sincerely thank Dr T. Warren Liao for providing me with invaluable guidance, constant encouragement and support throughout the course of my work. He has been very patient in explaining to me about writing a thesis. I have learned many valuable lessons from his teachings and our interactions in classroom and beyond.

I am indebted to Dr Bahadir K. Gunturk and Dr Pius J. Egbelu for accepting my request to be on the advisory committee. Both Dr Gunturk and Dr Egbelu have spared their invaluable time in giving comments and input in my work.

I would like to extend my special thanks also to Dr Jerry Draayer and Ms Hortensia Valdes, who have been very supportive and caring, in my first year at LSU. I would like to thank the Alton Ochsner Medical Foundation, New Orleans, who provided financial support to many Industrial Engineering graduate students, including myself.

Finally, I would like to express my heartfelt thanks to my friends- Chiranjit, Daada.

Table of Contents

List of Tables	iv
List of Figures	v
Abstract	vi
1. Introduction	1
1.1 Background.....	1
1.2 Research Objective	3
2. Literature Review.....	5
2.1 On Weld Extraction	5
2.2 On Weld Flaw Detection.....	8
2.3 On Image Segmentation	8
2.3.1 The Standard Hough Transform	9
2.4 On Fuzzy Sets and Membership Function	12
2.4.1 Entropy of fuzzy event	15
3. Methodology Overview.....	17
4. Binarization of Grayscale Image	19
4.1 Determining optimal parameter of S-function by Simulated Annealing	25
4.2 Formulation of optimization model and result of optimization model	28
5. Line Detection Using Standard Hough Transform.....	33
5.1 Finding line coordinates using SHT algorithm- Threshold based method.....	36
5.2 Finding line coordinates using SHT algorithm- Hough Peak based method	40
6. Fuzzy C-means For Clustering Lines Detected Using SHT Algorithm-Threshold Based Method	44
7. Post-Processing To Find Lines That Are Weld	47
7.1 Weld-peak detection for detecting weld location	49
7.2 Effects of changing ρ -axis cells in <i>Accumulator</i> array	54
7.3 Effects of changing the adaptive threshold in Houghpeak based method.....	55
8. Conclusion and Discussion of Results	57
Bibliography	59
Vita	62

List of Tables

Table 1 Optimization result of sample images found using simulated annealing, showing the fuzzy region (a, b, c), entropy, and binary thresholds.....	29
Table 2 Result of SHT algorithm-Threshold based method for sample images	38
Table 3 Output of SHT algorithm- Houghpeak based method of sample images.....	42
Table 4 Result of Clustering at C=10 for sample images.....	46
Table 5 Result of Threshold and Houghpeak based methods. Confusion matrix for 100 actual welds using 25 test images	54
Table 6 Confusion matrix for 100 actual welds at different ρ sub-divisions	55

List of Figures

Figure 1 (a) XY plane; (b) slope-intercept plane	11
Figure 2 A representation of Triangular MF	13
Figure 3 Example of a trapezoidal membership function.	14
Figure 4 Example of an S-function	14
Figure 5 Block diagram of our weld extraction process	17
Figure 6 Sample radiographic weld images.	19
Figure 7 a Histogram of sample images 1 and 2 in Figure 6.....	21
Figure 7 b Histogram of sample images 3 and 4 in figure 6	22
Figure 8 Binarization of sample images using global thresholding by Otsu [2]	23
Figure 9 Entropy plot of sample image, Image 1	25
Figure 10 a The S-function plot using parameter (a, b, c) for images 1 and 2 in Table 1	30
Figure 10 b The S-function plot using parameter (a, b, c) for images 3 and 4 in Table 1	31
Figure 11 Result of binary thresholding by Cheng et al [1], applied to sample images.	32
Figure 12 (a) (ρ, θ) parameterization of lines in XY-plane. (b) sinusoidal curves in $\rho\theta$ -plane; the point of intersection ρ', θ' correspond to the parameters of line joining (x_i, y_i) and (x_j, y_j) . (c) division of $\rho\theta$ -plane into accumulator cells.....	33
Figure 13 Position of 10 peaks in the Hough transform matrix of sample images.....	43
Figure 14 Clustering of objects in the ρ, θ vector using FCM toolbox of Matlab software	46
Figure 15 Intensity plot of line image at $X=50$, center = 218, left =208 and right= 228 of image 1	50
Figure 16 Summary of results of Threshold based method (a) Welds in image 1; (b) Welds in image 2; (c) Welds in image 3; (d) Welds in image 4.	52
Figure 17 Summary of results of Houghpeaks based method (a) Welds in image 1; (b) Welds in image 2; (c) Welds in image 3; (d) Welds in image 4.	53

Abstract

The process of joining metals is called welding. At times, selecting a poor quality material or improper usage of welding technologies may cause defects in welded joints. Some of these welded joints have to be tested nondestructively, because their failure can cause lot of damage, for instance in power plants. Radiography is a very common method for non-destructive testing of welds. It is done by certified weld inspectors who have knowledge about weld flaws, looking at the radiograph of the welded joint with naked eye. The judgment of the weld inspector can be biased; subjective, because it is dependent on his/her experience. This manual method can also become very time consuming. Many researches were exploring computer aided examination of radiographic images in early 1990's. With much advancement in computer vision and image processing technologies, they are being used to find more effective ways of automatic weld inspection. These days, fuzzy based methods are being widely used in this area too. The first step in automatic weld inspection is to locate the welds or find a Region of Interest (ROI) in the radiographic image [7]. In this thesis, a Standard Hough Transform (SHT) based methodology is developed for weld extraction. Firstly, we have done binarization of image to remove the background and non-welds. For binarization, optimal binary threshold is found by a metaheuristic –Simulated annealing. Secondly, we use SHT to generate the Hough Transform matrix of all non-zero points in the binary image. Thirdly, we have explored two different paths to find a meaningful set of lines in the binarized image that are welds. Finally, these lines are verified as weld using a weld-peak detection procedure. Weld-peak detection is also helpful to remove any non-welds that were remaining. We have used 25 digitized radiographic images containing 100 welds to test the method in terms of true detection and false alarm rate.

1. Introduction

1.1 Background

Testing is an activity done to look for defects in a product, to give assurance of product's quality to the customer. Inspection can be viewed as organized testing of the product done over time to ensure that it does not fail. Inspection applies to all industries: software, engineering, mechanical, business, military, real estate and many others. Failure of a product can happen at any time in its working lifetime. Failure of some products can cause more damage in comparison to some others. For example, failure of a pressure vessel can be more damaging when compared to failure of a motor. In the process of joining metals, called as welding, metal are heated which upon cooling forms a strong joint or weld. Defect in weld can occur because of selecting poor quality material or due to application of improper welding procedure [5]. The American Petroleum Institute (API) and American Society of Mechanical Engineers (ASME) have developed standard shapes and forms of common defects [3, 30]. Some of these defects like cracks, lack of weld penetration and lack of fusion have been classified by these bodies as unacceptable to continue operation [30]. Testing of welded joint in industries is carried out in two major ways: Destructive and Non Destructive Testing (NDT). Destructive testing is one where product is subject to tests until it fails. Non destructive testing is one where the product is not destroyed or preserved. Welded joints such as those in power plants are often being subject to non destructive testing because a failure in power plant can be catastrophic [3]. Our study focuses on the non destructive testing of welded joints. Different techniques of non destructive testing are: Radiographic, Visual, Dye penetrates and Ultrasonic [3]. Visual inspection can be carried out with good vision, proper lighting and knowledge about weld flaws. It is cost effective

and oldest technique to check the condition of weld. Radiography and ultrasonic are most widely used NDT methods in examining discontinuities in the critical engineering and construction components. Welded joint is most common critical area of any engineering component. Hence, industrial radiography is widely used to check the surfaces for weld flaws. In radiography technique, radiographs are produced by permitting x-ray or γ -ray to pass through the weld that is being inspected. The radiographs are viewed by certified inspector to interpret weld quality. The certified human inspector makes a decision about accepting or rejecting the weld based upon his knowledge and training. This conventional method is subjective, inconsistent, biased and also the method is time consuming and labor intensive [8]. Due to these problems, a computer-aided weld inspection system can be of great assistance to the human inspector in making consistent assessments. A significant number of researches in automatic weld inspection started in late 1980's or early 1990's. Liao and Ni [3] and Liao and Li [31] had developed an automated radiographic NDT system for weld inspection. According to them a weld inspection method will have three components: weld extraction, flaw detection and flaw type classification. Much research in the following years is intensified in either of these two areas, i.e. weld extraction or flaw detection.

Several efforts have been made in segmenting weld from the background: image processing based methods [3, 13, and 27]; fuzzy based methods [28, 4, and 6]. All the previous efforts devoted to weld extraction are significant to this research. They all emphasize that weld extraction is critical because the region within a weld has to be extracted before a defect detection algorithm can be applied. Locating the ROI can be achieved automatically or manually by looking at the radiographic image. With the recent developments in image processing and artificial intelligence, several tools are available to achieve this step without any human

interpretation at all. It is evident from the work of other researchers that in order to apply defect detection algorithms it is essential to properly extract the weld region from the image. Thus calling weld extraction as the crucial head-function of automatic weld inspection system would be appropriate.

1.2 Research Objective

The upcoming trend in industrial radiography is towards automatic weld inspection [30]. There have been several developments around the world in applying fuzzy reasoning and image processing to automatic weld inspection. This research intends to make a contribution in the area of automatic weld inspection by doing a study of applying Hough Transform in extracting welds from image. To the best of our knowledge, Hough Transform has not been widely applied to the weld extraction systems. In the area of flaw detection, Yazid et al [30] have used Circular Hough Transform for detecting circular discontinuities in welded joints. They had tested the system with 11 radiographic images and showed high successful classification of weld flaws. However, a higher number of sample images are needed to test the system. Also they did not include any methodology to remove or lower detection of ambiguous objects. Many attempts in weld extraction have successfully achieved 100% classification of welds. At the same time it is very highly unlikely that any system with 100% successful classification rate also has 0% false alarm rate [28]. It is obvious that these types of systems are very difficult to develop.

The three major techniques used in automatic weld inspection so far have been: image processing, feature extraction and pattern recognition [7]. In the computer vision and image processing fields, the problem of determining location of line has great significance. Hough Transform is most widely used to solve this problem within binary images [14]. Also, the segmentation of images from non-destructive testing is one major applications of image

thresholding [32]. Radiographic images have low contrast, non-uniform illumination and blurred edges making it challenging to segment the objects [28]. There are several algorithms for image thresholding and each has its own advantages and disadvantages. In this research, fuzzy entropy based method proposed by Cheng et al [1] is adopted for binarization of image. Using the foreground information of binary image, a Hough Transform is generated. We have explored two different paths to find a useful set of lines in the binarized image that can be weld. The algorithm for Standard Hough Transform method is in Rafael C Gonzales et al [10]. Finally, post processing step is also shown to lower false alarm rate and verify lines that are weld.

In summary, we have done automatic weld extraction using Hough Transform in following steps:

- ❖ Binarization of image using Cheng et al [1] method for image thresholding.
- ❖ Determining the lines in the binarized image using Hough Transform.
- ❖ Finding a meaningful set of lines that are weld.
- ❖ Post-Processing to find lines that are weld.

2. Literature Review

2.1 On Weld Extraction

Liao and Ni [3] observed that the intensity plot of a weld looks more like Gaussian than any other object in the image. The extraction of weld was based on this observation. They divided the radiographic image into 4 sub images such that each sub-image contains one weld. Further in each sub-image, peak detection was used to extract the object. The objects can be weld and non-weld and the weld is defined as one with the lowest Mean Square Error (MSE). The method of weld extraction was tested with 25 radiographic images. Their method was able to do 100% successful classification of weld. They had also made a point that weld extraction has to precede detection of defect. Finding the ROI before doing flaw detection will reduce time and also make the process of weld inspection fully automatic in true sense. However, their method cannot be applied directly to tilted weld; it may not work, because intensity profile of tilted weld may not look like Gaussian. So it is essential to have the knowledge of weld angle. Also, a weld which was reworked or has defects in them will also not have Gaussian like shape. Another methodology is needed in cases where weld's intensity profile is not having Gaussian like distribution [13, 27]. Also in their method previous knowledge of the number of welds in the image is required which has to be done manually.

Using the image segmentation techniques can be effective in isolating weld region from background and non-weld if the quality of image is good. Ideally, in a good quality radiographic image the intensity value of weld region will be higher than its surrounding. However, the parent metal might absorb radiation differently on both sides of the weld thus the overlapping with intensity values of weld [27]. So it becomes extremely difficult to choose one threshold that will

separate weld and non-weld. Liao and Tang [4] say that it is not possible to completely extract welds based on multi-level image thresholding. Since the graylevel of some welds are overlapping with the gray-level of the gaps between two films strips making it difficult to choose a threshold value that will separate weld and non-weld. They extract four features from the objects in the line image using peak detection algorithm. After feature extraction is done a Multi-layered perceptron (MLP) based classification is used to separate weld and non-weld. The noise and discontinuities is rectified by post processing method. Firstly, Liao et al [6] used the similar approach for extracting features. Secondly, they have used fuzzy K-NN and fuzzy c-means algorithm for pattern classification and have compared the performances of both approaches. A post processing step is introduced to lower false alarm rate [6].

Lim, Ratnam and Khalid [27] have proposed an approach for weld bead extraction using gray level intensity information across the weld. They use the maximum intensity of the intensity profile as the center and divide in two parts. In each part, least square lines were fitted to its data points using a predefined range threshold of 3 to 6. The weld bead boundary points on each part are found using error threshold.

Two more recent works in weld extraction are based on fuzzy reasoning [7 and 28]. Liao [7] develops a fuzzy reasoning based expert system for weld recognition. According to Liao [7] a fuzzy reasoning method will contain: pattern matching, aggregation of antecedents, implication operation, aggregation of rule outputs and de-fuzzification. Three features are extracted of each object: object width, MSE of intensity profile and peak gray-level. The optimal number of fuzzy terms of each feature and their shapes are determined with fuzzy c-mean based on MSE criterion [29]. The MSE is calculated by fitting the domain value and membership value to some commonly used functions to be described in Section 2.4. The weights have been assigned to each

rule based on max-min composition and mean-min composition. The performance of this optimal rule set is tested against other combination of terms based on its accuracy, false positive rate (non-weld mistaken as weld) and false negative (weld mistaken as non-weld). Liao [7] is the first in weld recognition using fuzzy reasoning.

The two features used in fuzzy reasoning by Ou and Song [28] are local spatial contrast (C) and local spatial variance (V). They have defined

$$V(i, j) = \frac{1}{m * n - 1} \sum_k^m \sum_{l=1}^n (x_{k,l} - A(D))^2$$

Where D consists of $m \times n$ pixels and centers at (i, j) , $x_{k,l}$ is the gray level value of pixel (k, l) and $A(D)$ is the average value of region D. The spatial contrast, $C(i, j)$ has been defined by them as $C(i, j) = A(D) - A(E)$, where $A(D)$, $A(E)$ are the average value of region D and E respectively and the number of pixels between D and E is n .

They have used the Wang and Mendel's method for generating fuzzy rules using input data pairs. The number of input or features are two, spatial contrast and spatial variance. The output is membership value $F(i, j)$ which is used to determine if pixel at i, j is edge point. They tested with 101 radiographic images having 153 welds (determined by visual examination). Their method could successfully classify 141 welds.

Computational vision can also be directly applied to detect weld flaws from radiographic images. The segmentation of weld flaw shape and its features could be used in pattern classification. These types of methods do manual selection of the weld region by visual examination. Some of the work in this area is discussed in next section.

2.2 On Weld Flaw Detection

Wang and Wong [8] propose an automatic-vision system for weld flaw detection based on image segmentation. Selecting an optimum threshold that will separate weld defects from background is difficult because the defects have low contrast and noise is present in the weld region. Nevertheless, weld defects can be extracted by combining digital image processing techniques. The first step in that is improving quality of the radiographic image by reducing its noise (adaptive wavelet thresholding) and enhancing its contrast (contrast limited adaptive histogram equalization). Wang and Wong [8] show that applying three level thresholding to the enhanced image can separate weld defect from the background. Although their paper is in direct weld flaw detection, it is relevant to thresholding step of this research.

Different types of weld flaws can have different shapes; however, one particular type of discontinuity will have its circular shape. Yazid et al [30] have done circular discontinuities detection using Circular Hough transform. They have found edge of weld using Sobel edge detector. Before edge detection, preprocessing of image is done to improve contrast of image. Several other steps before applying Circular Hough Transform are: defect segmentation, noise reduction and severability filter. Finally an object having circular shape is detected and classified by Hough Transform as weld defect.

2.3 On Image Segmentation

Image segmentation is an important path to extracting information from images. Autonomous image segmentation is one of the most difficult tasks in image processing. In general, there are two popular categories of approaches to the problem posed by image segmentation. In the first

category is detection of line, edge, isolated points and the second category is thresholding, region splitting, region splitting and merging, Rafael C Gonzales et al [10]. It is essential in image thresholding to be able to select appropriate threshold of gray level for extracting objects from background. Otsu [2] proposed a simple procedure using information from gray-level histogram of the image for image thresholding. The image information's that can be exploited in image thresholding are: histogram shape, entropy, object attributes and local gray-level surface [32]. The classical approach of image segmentations; thresholding, edge detection, line detection can also be achieved using fuzzy theory approach [24]. Many image properties such as boundary, region, and brightness are ambiguous in nature. Fuzzy set theory has been successfully used in handling such properties in image processing. Also, the transformation of graylevel representation of image to another should make the solution to the analysis problem easier [23].

In both natural and man-made objects there appear straight lines and so the problem of determining their location and orientation is of great importance in computer vision and image processing. Hough Transform is a conventional method to find lines in binary images. The Hough transform consists of (1) computing gradient of image, (2) specifying subdivisions in $\rho\theta$ plane, (3) examining the counts of the accumulator array or Hough transform matrix for high pixel concentrations and (4) examining the relation between pixels in a chosen cell. Agarwal and Karl [14] have also addressed the problem of finding lines in grayscale images. Their work has not been widely explored by researches for industrial radiography applications.

2.3.1 The Standard Hough Transform

Consider an image with n pixels. These pixels can be thought of as n points lying in the image space. There can be any number of lines passing through a point. One possible solution is to find

all lines determined by every pair of points. This solutions involves finding $C(n,2) \sim n^2$ lines and then performing $n \times C(n,2) \sim n^3$ comparisons of every point to all lines. This solution is practically infeasible because of computation complexity. The Hough transform is a simplified method to find the subset of the n points that lie in a straight line. The equation of a straight line is given below,

$$Y_i = aX_i + b. \quad (1)$$

Where, (X_i, Y_i) is a point on the line, a is slope of line and b its intercept.

In the XY plane there can be infinite number of lines passing through (X_i, Y_i) that satisfy the equation (1). Rewriting the equation (1) as $b = -X_i a + Y_i$ and considering the slope-intercept plane we get the equation of single line for a fixed pair of (X_i, Y_i) . Moreover, another point (X_j, Y_j) also has a single line in the slope-intercept plane and these two lines intersect each other at point (a', b') . So (a', b') becomes the slope and intercept of a single line in the XY plane that contains both these points (X_i, Y_i) and (X_j, Y_j) . The illustration of this concept is shown below in Figure 1.

In Hough transform, an accumulator array (or Hough matrix), A , is created of the expected range of slope and intercept values, the range of slope is $(a_{min} \ a_{max})$ and intercept is $(b_{min} \ b_{max})$. Then for every point, (X_k, Y_k) , we let the slope parameter to take each value in the assumed range and solve for the intercept. If a choice of slope, a_p results in intercept, b_p , within their allowed ranges then the value of $A(p, q)$ is incremented by 1. This step is repeated until all the possible slopes from a_{min} to a_{max} be exhausted. At the end of this procedure each cell value in the accumulator array will correspond to the number of points lying on a line, the slope and intercept of which could be found.

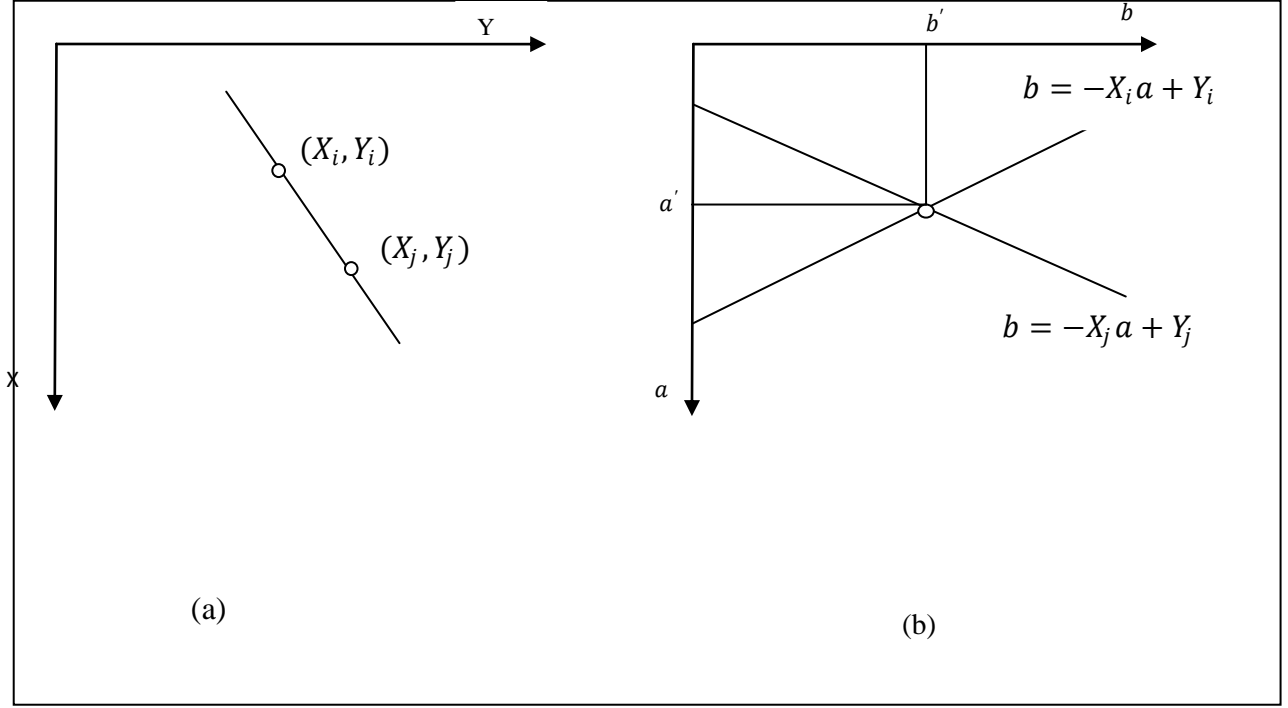


Figure 1 (a) XY plane; (b) slope-intercept plane

A threshold value can be set which give the minimum number of points that will form a line. Any value in the accumulator cell which is greater than the threshold value can be qualified. Another approach for qualifying cells from the accumulator array is finding peaks or maximum in the array. Finding a meaningful set of the cells with maximum values in the accumulator array is challenging. It is discussed in detail in Chapter 5. Thus we can determine the slope and intercept of the possible lines in any image using Hough Transform. However, in the Equation (1) as the line approaches vertical, the slope and intercept approach infinity. To avoid this difficulty during calculations in the Standard Hough transform we use the normal representation of line. The normal form of the equation of a straight line is given below,

$$x \cos \theta + y \sin \theta = \rho \quad (2)$$

Where θ or theta is angle with x-axis and ρ or p or rho is the perpendicular distance from origin.

The range of angle θ is $\pm 90^\circ$ with respect to x-axis.

2.4 On Fuzzy Sets and Membership Function

In nutshell, the notion of sets is the classification of objects which share the same properties into one class. In Set theory, $A = \{x \mid x \in X\}$ is a set in the universe of X . Basically, x satisfies some property which uniquely defines A . For example, $A = \text{Students in IE-101 class}$; $X = \text{LSU graduate students}$. Characteristic function $A(x)$ can then be defined by equation (3):

$$A(x) = \begin{cases} 1, & \text{if } x \in A \\ 0, & \text{if } x \notin A \end{cases} \quad (3)$$

Contrary to regular sets, fuzzy sets allow us to accept or reject to a certain degree. Whether an object belongs to a certain class is expressed by real number in the unit interval $[0, 1]$. A fuzzy set is characterized by a membership function mapping the elements of a domain, space or universe of discourse X to the unit interval $[0, 1]$. That is $A: X \rightarrow [0, 1]$, Zadeh [25]. Mostly, the categories we use in describing real-world objects do not have well-defined boundaries. For instance, a certain age group that define a young man or a old man can be called ambiguous or fuzzy. In image processing, many definitions such as edge of any object is fuzzy in nature. To define such kind of notions that are fuzzy in nature, we use Membership Functions (MF) instead of characteristic function. Some very common MF's are Triangular, Trapezoidal and S shaped membership function. The equation for determining degree of membership in Triangular membership function is given by equation (4):

$$\tilde{A}(x_0; a, b, c) = \begin{cases} \frac{x_0 - a}{b - a}, & \text{if } a \leq x \leq b \\ \frac{c - x_0}{c - b}, & \text{if } b \leq x \leq c \\ 0, & \text{otherwise} \end{cases} \quad (4)$$

A triangular membership function is shown in Figure 2 below. In Figure 2, b is the modal value and a, c denote the lower and upper bounds respectively. The degree of membership $A(x_0)$ given by the Equation (4) for any x between a, c is a real number between 0 and 1. The degree of membership is 0 for any other values of x outside of the bound $[a, c]$.

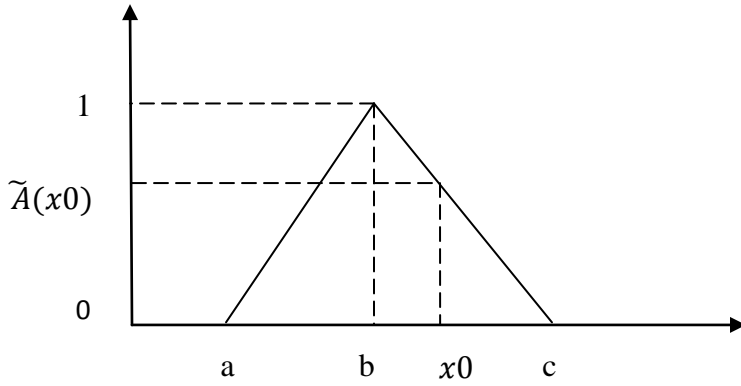


Figure 2 A representation of Triangular MF

The equation for determining degree of membership in Trapezoidal membership function is

$$\text{given by equation (5): } \tilde{A}(x; a, b, c, d) = \begin{cases} \frac{x - a}{b - a}, & \text{if } a \leq x \leq b \\ 1, & \text{if } b \leq x \leq c \\ \frac{d - x}{d - c}, & \text{if } c \leq x \leq d \\ 0, & \text{otherwise} \end{cases} \quad (5)$$

The trapezoidal membership function is shown in Figure 3 below. The degree of membership $A(x)$ given by Equation (5) for any x between b and c is 1. The degree of membership for any x outside of bound $[a, d]$ is 0.

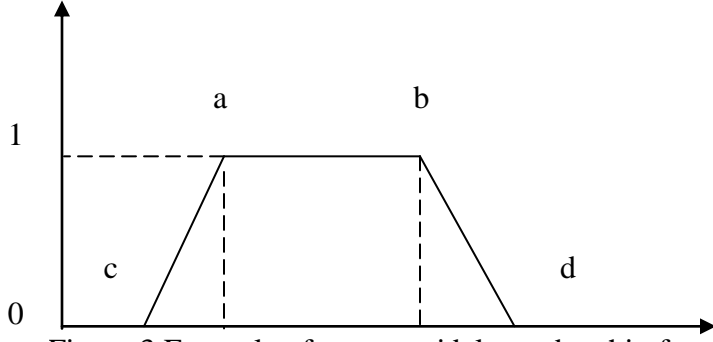


Figure 3 Example of a trapezoidal membership function

The equation for determining degree of membership in S membership function is given by equation (6):

$$\tilde{A}(x; a, b, c) = \begin{cases} 0, & \text{if } x \leq a \\ \frac{(x-a)^2}{(b-a)(c-a)}, & \text{if } a \leq x \leq b \\ 1 - \frac{(x-c)^2}{(c-b)(c-a)}, & \text{if } b \leq x \leq c \\ 1, & \text{if } c \geq x \end{cases} \quad (6)$$

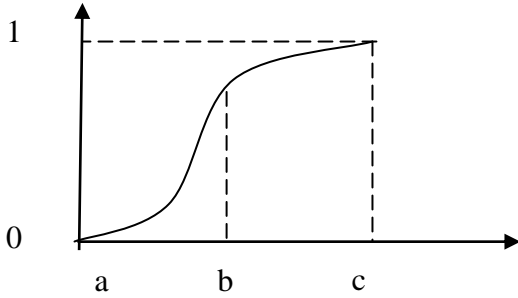


Figure 4 Example of an S-function

The S membership function is shown in Figure 4. Suppose variable x is the gray level of the pixels in a grayscale image then the lower and upper bounds will be 0 and 255. Cheng et al [1] used S membership function to convert the image from gray-scale to fuzzy domain for image thresholding. In Equation 6, a , b , c are three parameters which determine the shape of S membership function.

2.4.1 Entropy of fuzzy event

The definition of a fuzzy term, meaning finding the degree of membership, is the first step in solving any problem using the concept of fuzzy set theory. The most commonly used fuzzy terms have been discussed in the previous section, section 2.4. Liao et al [29] proposed a method to determine fuzzy terms based on a variant of the fuzzy c-means algorithm. Cheng and Chen [19] and Cheng et al [1] have applied the fuzzy entropy principle to define the S membership function for image processing applications.

The entropy of fuzzy event is the entropy measure of fuzziness. Consider variable X with a finite number of outcomes x_1, x_2, \dots, x_n and their probabilities p_1, p_2, \dots, p_n . The sum of all probabilities is 1. Shannon and Weaver (1949) introduced the concept of entropy and they defined entropy as:

$$H(p_1, p_2, \dots, p_n) = \sum_{i=1}^n p_i \log_2 p_i. \quad (7)$$

According to information theory, Rafael C Gonzales et al [10] the large the entropy the more information is contained or associated with the source. Cheng et al [1] proposed a new formula for calculating the entropy of a fuzzy set. They take into consideration the membership of each element and the probability distribution. Cheng's equation for fuzzy entropy is given below in Equation (8):

$$H(A, N, mf_A) = -1/\log N \sum_{i=1}^N P_p(A_i) \log P_p(A_i) \quad (8)$$

The term $P_p(A_i)$ in Equation (8) is the probability sum of those x mapping into A_i by the membership function mf_A .

The advantage of this new entropy formula is discussed in details in their paper - Cheng et al [1]. The selection of a membership function is done according to the application. In the above Equation (8), the number of partitions N can be changed according to the application. The term P_p can be determined from the histogram of image. So, if the value of N is fixed, the output of Equation (8) will depend on the membership function.

If the S membership function is chosen for finding mf_A then equation (8) can be rewritten as:

$$H(A, a, b, c) = -1/\log N \sum_{i=1}^N P_p(A_i, a, b, c) \log P_p(A_i, a, b, c) \quad (9)$$

The problem is to find a combination of (a, b, c) such that H (A, a, b, c) has maximum value. There are some metaheuristic methods like genetic algorithm, ant colony optimization, simulated annealing that can be used to solve the problem. Cheng et al [1] have used genetic algorithm for finding optimal values of (a, b, c) and also showed its application for image thresholding and image enhancement.

3. Methodology Overview

To achieve the objective set forth for this research, a methodology was developed. The step by step methodology is shown as block diagram in Figure 5.

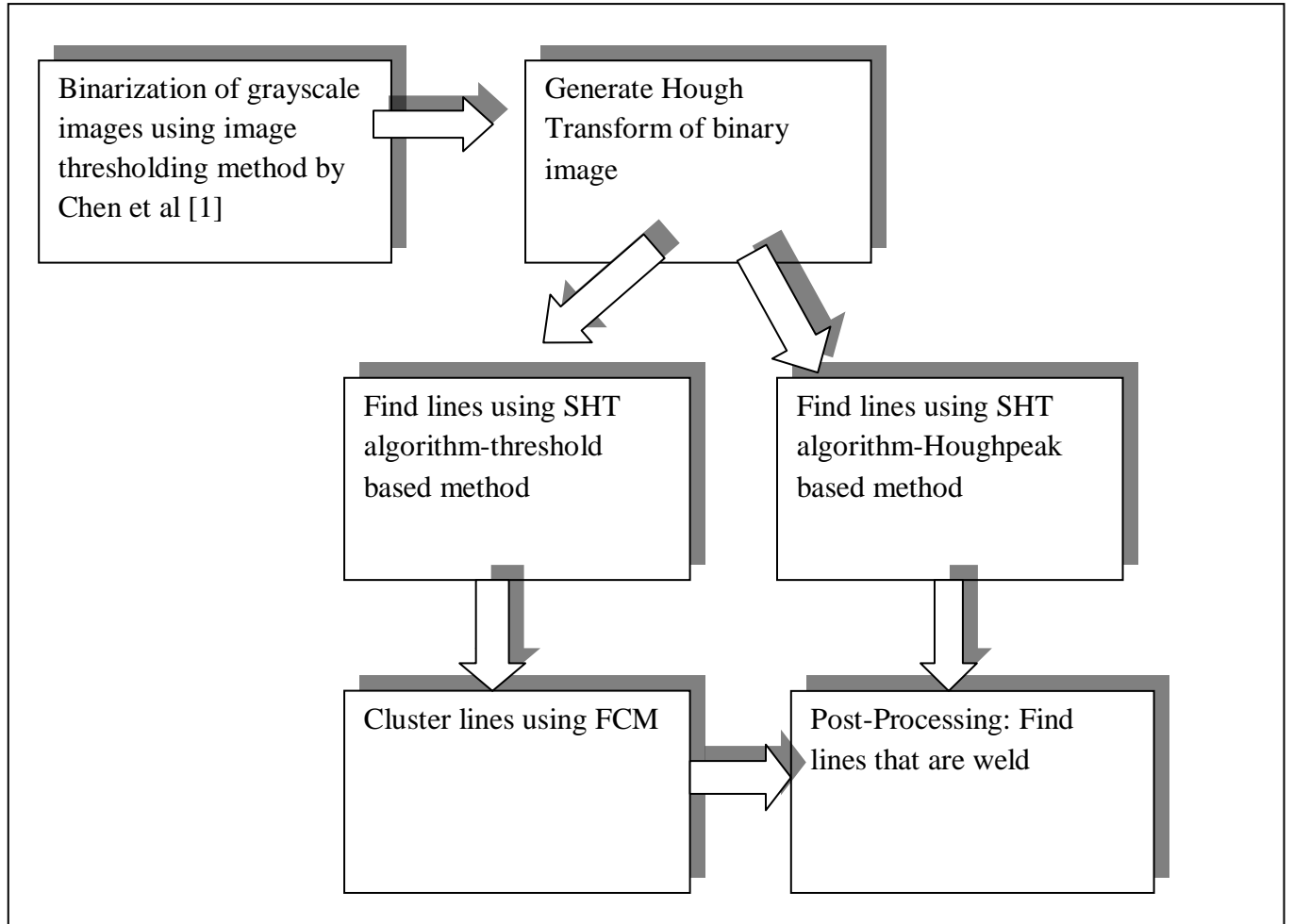


Figure 5 Block diagram of our weld extraction process

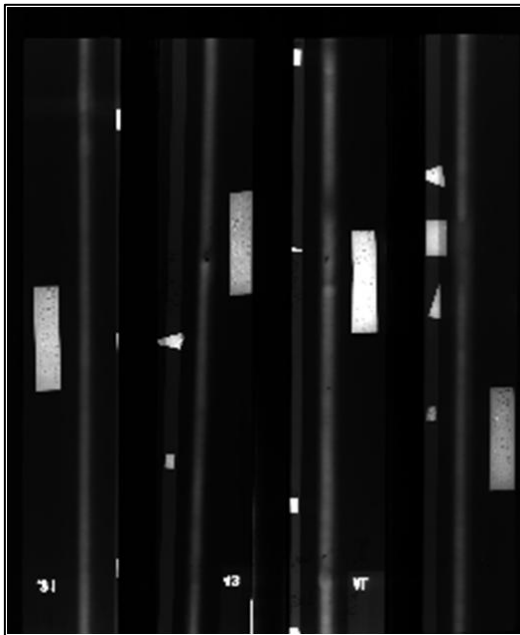
The first step is binarization of the grayscale radiographic images. The method adopted for binarization of images is the fuzzy entropy principle based method of Cheng et al [1]. A computer program was written in Matlab software to replicate their method using the same

process conditions as given in their paper. The first task was running the computer program for 20 times and recording the output in each run. The output recorded during each run was: S-function parameters (a, b, c) and entropy. For each output, one threshold value was determined as described in their paper. The best of 20 threshold value was chosen for converting the grayscale image to binary image. All the pixel intensities in the image equal to or greater than threshold value will take the value 1 and others would be 0. This method for binarization was repeated for 25 grayscale images to obtain 25 binary images.

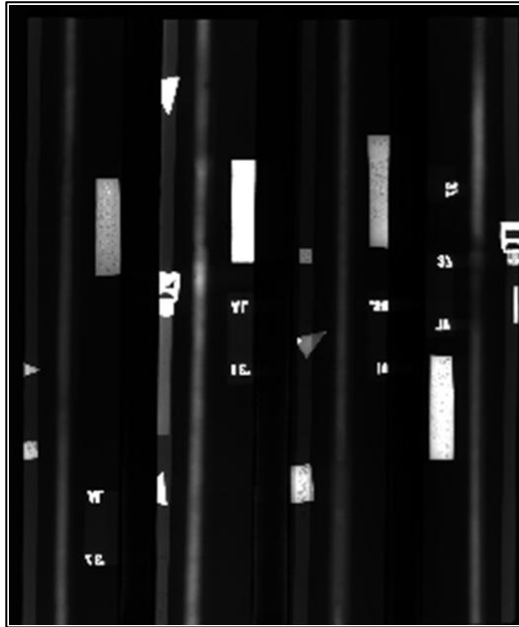
The second step is determining the position of lines in the binarized image using SHT. We have tried two different paths to find lines using SHT algorithm, threshold based and Houghpeak based method. A computer program using Matlab software was used to find lines using SHT algorithm-threshold based method. The lines detected using threshold based method is grouped into 4, 5, 6, and 10 lines using Fuzzy C-means. The image processing toolbox of Matlab software was used to find lines using SHT algorithm-Houghpeak based method. Finally, a post-processing procedure is used to find the lines that are weld. We have called it, weld-peak detection algorithm. All the computer programs were developed in Matlab environment. The computing resource used was 2 GHz Intel Core 2 Duo CPU with 4 GB of random access memory.

4. Binarization of Grayscale Image

The four sample grayscale images used in this thesis, called image 1, 2, 3, and 4, are shown in Figure 6.



(a) Image 1



(b) Image 2



(c) Image 3



(d) Image 4

Figure 6 Sample radiographic weld images

The above shown images are each 250 pixels by 300 line image. The image contains several reference objects like rulers, penetrometers, densitometers, identification letters, and space between weld strips. The shape of the weld is of interest and it has to be preserved in the process of binarization. The 25 images used in this thesis are the same as in the paper, Liao and Ni [3]. The details of acquiring radiographic images and converting to grayscale image are discussed in their paper. They called it, Probability of Detection (POD) tape and used 25 POD tapes, each containing down-sampled image, which is the 250- pixel by 300 line image shown in Figure 6. Traditional image processing techniques are less effective with radiographic images because they have low contrast, blurred edges and non-uniform illumination [28]. To test the working of simple thresholding method [2], the histograms of the images in Figure 6 are created, as shown in Figure 7a and 7b.

Looking at the histogram of images, it is not easy to select a single threshold using global threshold, T . The image must be having light objects in a dark background so it can be easily grouped into two dominant modes by selecting a threshold. To demonstrate that traditional image processing methods will not work for radiographic images, we did global thresholding by Otsu [2]. The global threshold, T for sample image 1, 2, 3, and 4 was determined as 93, 108, 131.5, and 120 respectively. All pixel labeled as 1 correspond to objects having gray level intensity larger than T . The result of applying Otsu [2] to image 1 is shown in Figure 8. It can be observed from Figure 8 that weld objects are removed while non-weld objects are retained, which is not desirable for weld extraction.

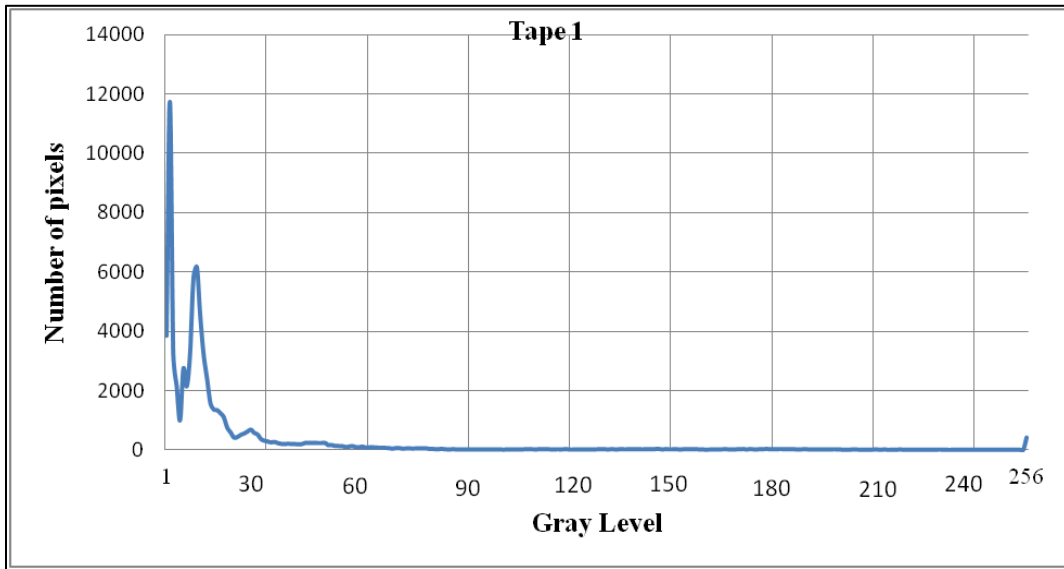


Image 1

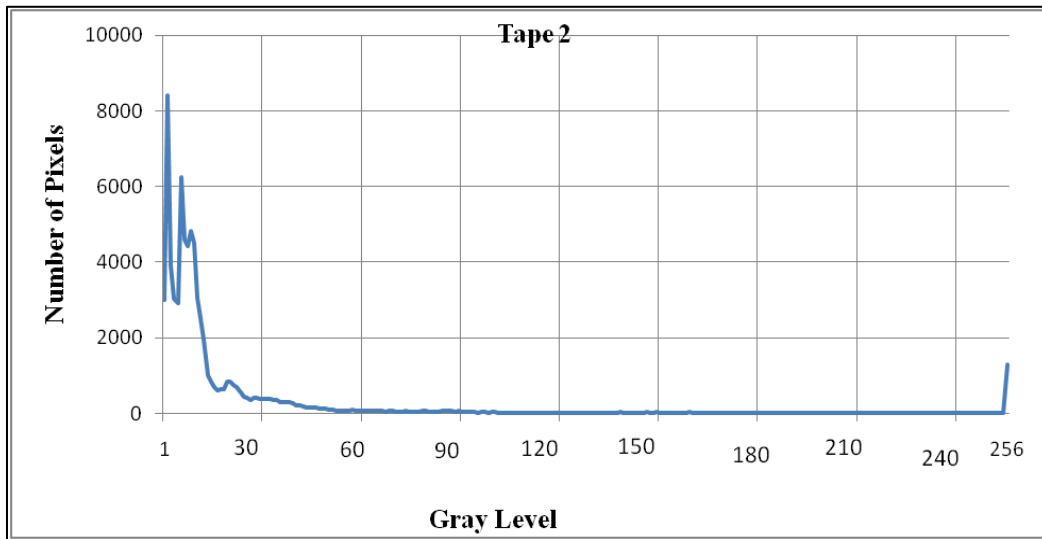


Image 2

Figure 7 a Histogram of sample images 1 and 2 in Figure 6

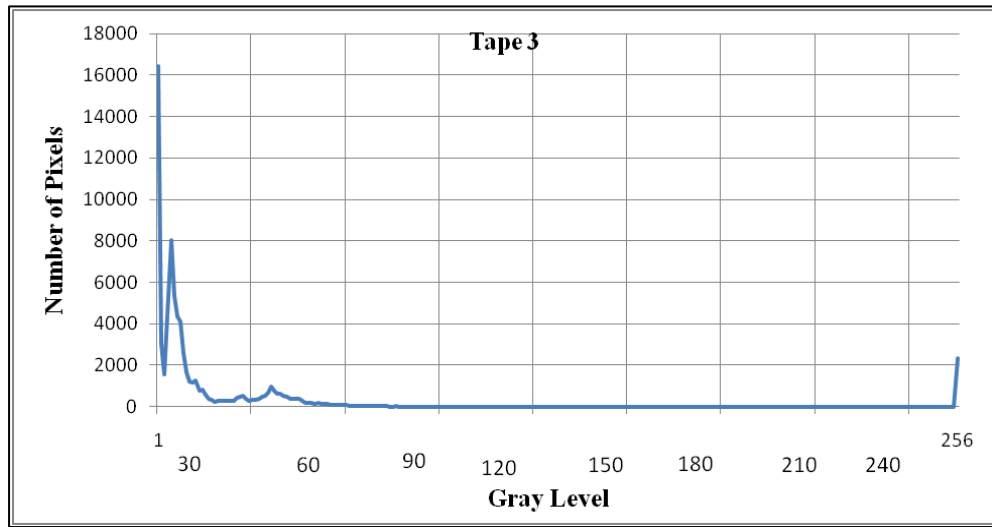


Image 3

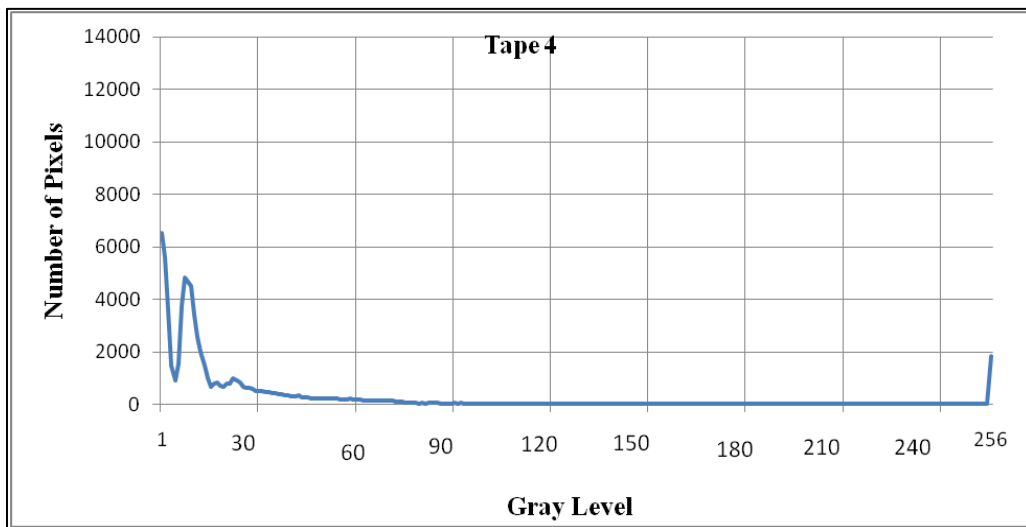
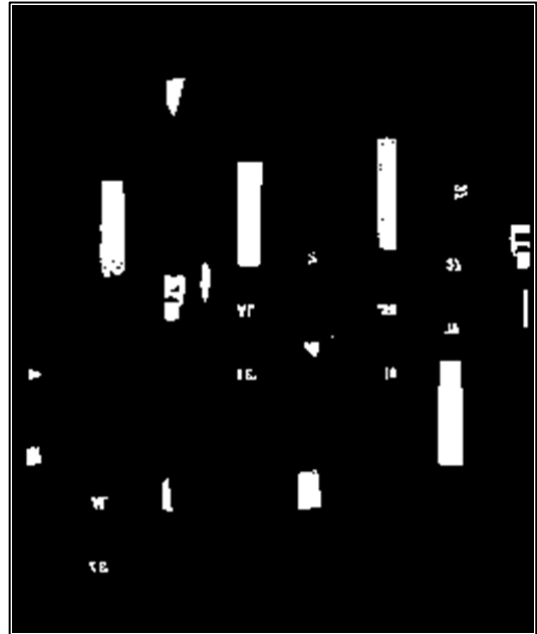


Image 4

Figure 7 b Histogram of sample images 3 and 4 in figure 6



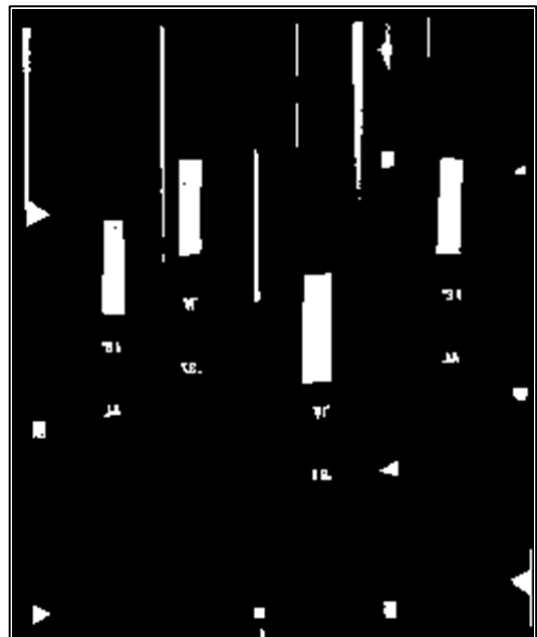
(a) Image 1



(b) Image 2



(c) Image 3



(d) Image 4

Figure 8 Binarization of sample images using global thresholding by Otsu [2]

We have applied a more robust fuzzy entropy based method for binarization [1]. This section will cover in detail the binarization of grayscale image done in our research. As mentioned earlier in section 2.4.1, the objective is to find the optimal parameters of S-function that maximize entropy. The entropy can be calculated using Equation (9). However, there are two features that are dependent on the application: number of partitions, N and partition method. So, if we want to classify a given image into five categories (A1, A2, A3, A4, and A5) say equivalent to (Very Dark, Dark, Medium, Bright, and Very Bright) by equal partition method. We can divide interval [0, 1] into 5 equal sub intervals [0, 0.2], [0.2 0.4], [0.4 0.6], [0.6 0.8], and [0.8, 1.0] to represent A1, A2, A3, A4, and A5 respectively. The term, $P_p(A_i, a, b, c)$ and can be determined by dividing the number of pixels in A_i mapped using S-function by 75000 (as per input image, 250 pixel \times 300 line). The histogram of image 1, 2, 3, and 4 are shown in Figure 7a and 7b.

The maximum pixel intensity of sample images is 255, and the minimum is 0. So 0 and 255 are the lower and upper bounds to this maximization problem. If N=5 then Equation (9) can be rewritten in Equation (10) as below:

$$H(A, a, b, c) = -1.4307 \sum_{i=1}^5 P_p(A_i, a, b, c) \log P_p(A_i, a, b, c) \quad (10)$$

We have used the equation (10) as the final objective function for maximization using generalized simulated annealing for function optimization by Bohachevsky et al [9]. Figure 9 shows the entropy plot of sample image 1 using Equation (10). The entropy function is fitted with smooth surface using ‘gridfit’ [33].

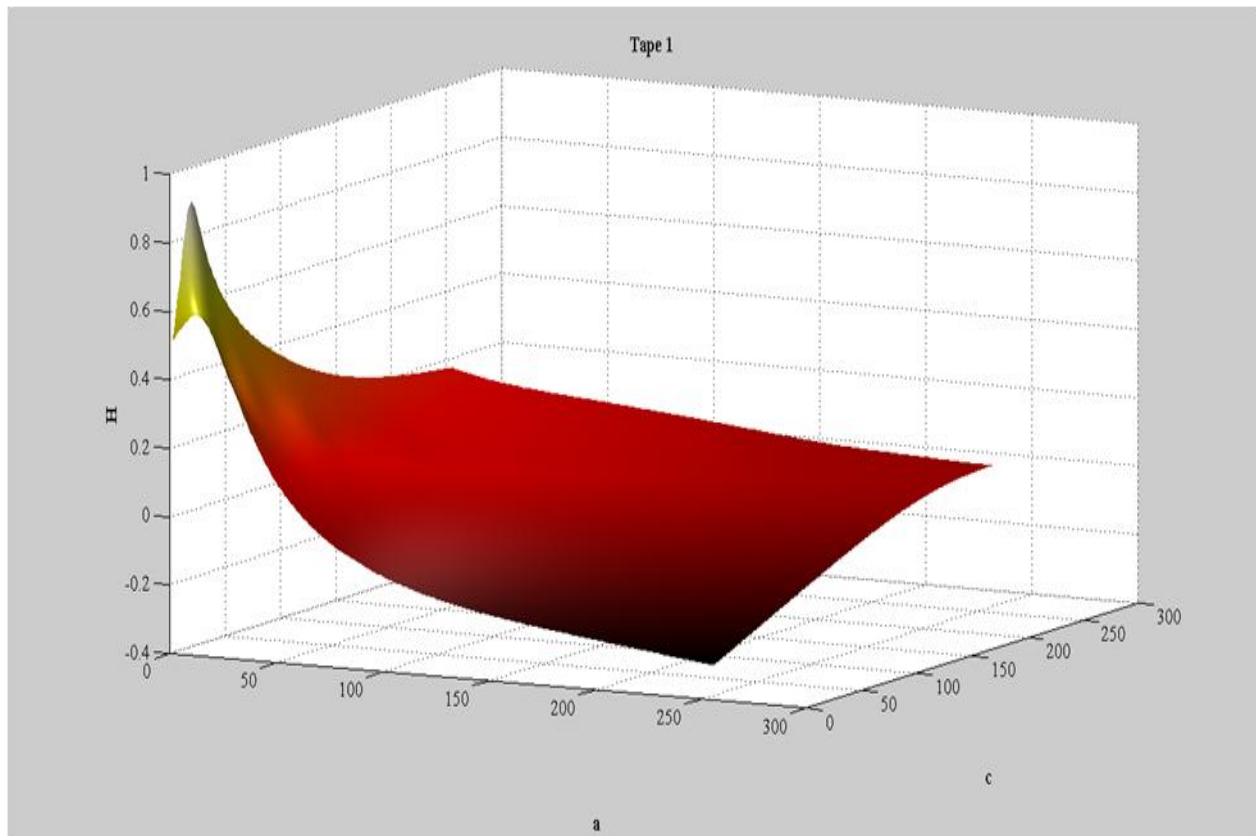


Figure 9 Entropy plot of sample image, Image 1

The global maximum value of plot is 0.9854, located at $a=0$, $b=2$, and $c=32$. The b value is not shown in Figure 9 because it is difficult to plot 4 dimensions.

4.1 Determining optimal parameter of S-function by Simulated Annealing

The Simulated Annealing (SA) algorithm is a general optimization technique for solving combinatorial optimization problems. SA is the mathematical model of annealing process of metals. In physical annealing process, the atoms of molten metal tend to take relative positions to reach a state of minimum energy when cooled to freezing temperature. So Simulated Annealing algorithm is very efficient in minimizing a certain function, Bohachevsky et al [9]. SA algorithm is very much like any simple heuristic for local search. SA algorithm starts with a randomly

chosen initial solution then a neighbor of this solution is generated by some simple computation. The costs associated with current solution and neighbor solutions are calculated. If the change in cost due to the neighbor solution is reduced then it is accepted as the current solution. So far the SA algorithm is similar to any local search algorithm. The difference from any local search method is that in SA algorithm an undesired solution can also be accepted as the current solution based on a controlled probability factor, Koulmas et al [16]. Our implementation follows the generalized simulated annealing for function optimization proposed by Bohachevsky et al [9]. The pseudo code of the implemented simulated annealing algorithm is given below assuming the objective function as maximization function.

Step 1: Initialize parameters which include maximum temperature: $TMAX$, minimum temperature: $TMIN$, cooling rate: $ALPHA$, maximum number of iterations: $MAXITR$, step size: DR , a parameter, g .

Step 2: Randomly generate a solution, X and evaluate the objective value, OBJ . Let this solution be the current solution, X_CUR and the best solution, X_OPT up to this point. Also, let the best objective value, OBJ_OPT and current objective, OBJ_CUR be same as OBJ .

Step 3: Set the Current temperature, $T=TMAX$ and Iteration counter, $I = 1$.

Step 4: **WHILE** $T > TMIN$

a. **WHILE** $I \leq MAXITR$

i. Update solution, $X = X_CUR + DR \times (U) \times (1 - I / MAXITR)$, with U being a standard normal variate.

- ii. Update objective value, OBJ of new solution
- iii. Calculate change in objective value, $DELTA = OBJ - OBJ_CUR$
- iv. Calculate probability of accepting the solution according to equation (11)

as given below:

$$P = e^{-\left(\frac{DELTA}{T}\right)^g} \quad (11)$$

- v. Update the current solution X_CUR and current objective OBJ_CUR if $DELTA$ is positive value OR $P < rand$, where $rand$ being a uniformly distributed random value $\in [0, 1]$.
- vi. Increment iteration counter by one.

END WHILE

b. **IF** $OBJ_CUR > OBJ_OPT$, update the best solution X_OPT and the best objective value OBJ_OPT .

c. Update the current temperature, $T = T \times ALPHA$

END WHILE

Step 5: Output the result of optimal solution and its objective value.

Major parameters associated with SA algorithm include maximum temperature, $TMAX$, minimum temperature, $TMIN$, cooling rate, $ALPHA$, a parameter that defines how fast or slow the cooling happens, maximum number of iterations: $MAXITR$, a parameter that controls the number of iterations during each step of cooling, step size: DR , a parameter that calculate the neighbor solution (step size gradually reduces as the algorithms converges to the best solution),

g , an arbitrary negative number. For this study, they are fixed at 1, 0.001, 0.95, 20, 63.75 ($=0.25 \times 255$), and -2 respectively.

4.2 Formulation of optimization model and result of optimization model

We formulate the optimization model as follows:

$$\textbf{Maximize}, H(A, a, b, c) = -1.4307 \sum_{i=1}^5 P_p(A_i, a, b, c) \log P_p(A_i, a, b, c)$$

$$\textbf{Subject to}, 0 \leq a \leq b \leq c \leq 255$$

We have employed $N = 5$ and equal partition. So according to equal partition, after determining the object function, constraints and all SA parameters, SA can find the solution (a, b, c) with the maximal entropy $H(a, b, c)$. Now, we apply the proposed approach to image thresholding. We observed that the result was not same each time we run the SA algorithm. So, we run the SA algorithm 20 times to generate sufficient statistical data. The best, medium and worst objective values are recorded along with optimal solutions. Table 1 summarizes the optimization results by simulated annealing for four sample images, image 1, 2, 3, and 4. We have chosen to use the best solution of the optimization results. After selecting S-function parameters, (a, b, c) , the images are mapped into fuzzy domain and partition point is found. For instance, the best objective value of $H(A, a, b, c)$ of image 1 is 0.9854. The performance of simulated annealing algorithm can be illustrated in Figure 9. Figure 9 shows the objective function has global maximum at $a=0$ and $c=32$. The value of global maximum for sample image 1 is 0.9854. The best optimal solution found by simulated annealing in 20 runs (given in Table 1) was (0, 2, and 32). The best solution of 20 run for sample image, image 1 found by simulated annealing is the global optimum. From this we learn that simulated annealing performs very well.

The performance of SA algorithm largely depends on probability of accepting an inferior solution in iteration; P , found using equation (11). If P is too close to 1 or below 0.5, the search becomes less efficient. It is best to keep its value between 0.50 and 0.9 [9].

Table 1 Optimization result of sample images found using simulated annealing, showing the fuzzy region (a, b, c), entropy, and binary thresholds

		Image 1	Image 2	Image 3	Image 4
Objective value	Best	0.9854	0.9943	0.9966	0.9670
	Median	0.9761	0.9905	0.9551	0.9547
	Mode	0.9794	0.9943	0.9551	0.9576
	Worst	0.9686	0.9805	0.9493	0.9411
Best Optimal solution		(0, 2, 32)	(1,3,21)	(0,1,16)	(0,2,32)

The optimal solution from Table 1 was used to plot the S-function. Figure 10 a and 10 b shows the S-function plot for parameters (a, b, c) which is the best optimal solution. The partition point in the fuzzy domain is where membership degree is 0.85. The partition point when mapped back to graylevel using inverse S-function has given us the single threshold for binarization purposes.

The binary thresholds found using simulated annealing for sample images; image 1, 2, 3, and 4 are 21, 15, 11, and 21 respectively. Figure 11 summarizes the result of binarization of sample images. It can be observed that fuzzy entropy based binary threshold [1] is very efficient in retaining welds unlike binary threshold by global threshold [2].

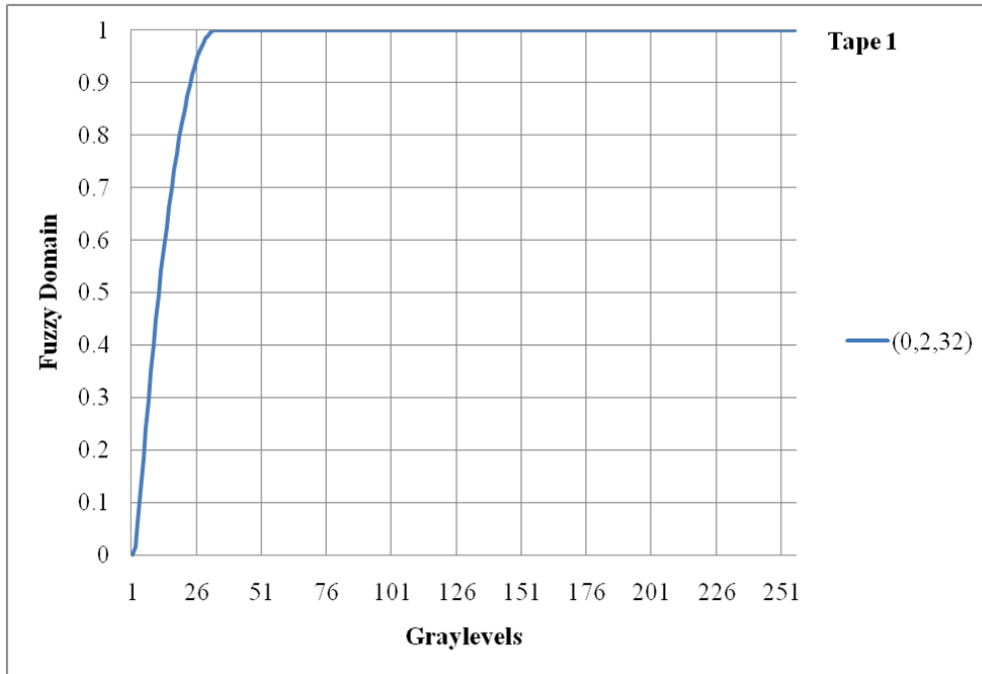


Image 1

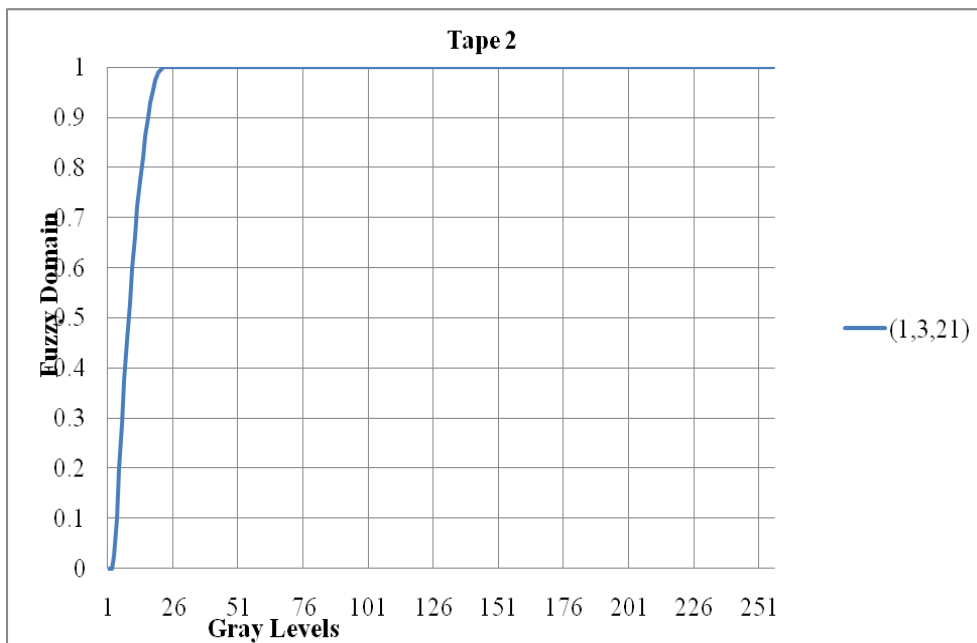


Image 2

Figure 10 a The S-function plot using parameter (a, b, c) for images 1 and 2 in Table 1

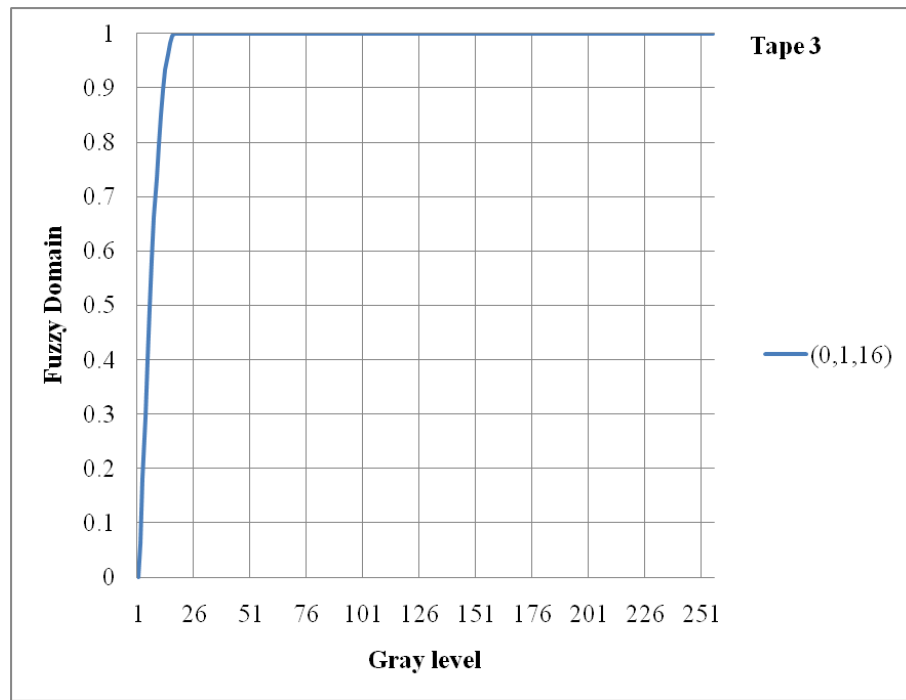


Image 3

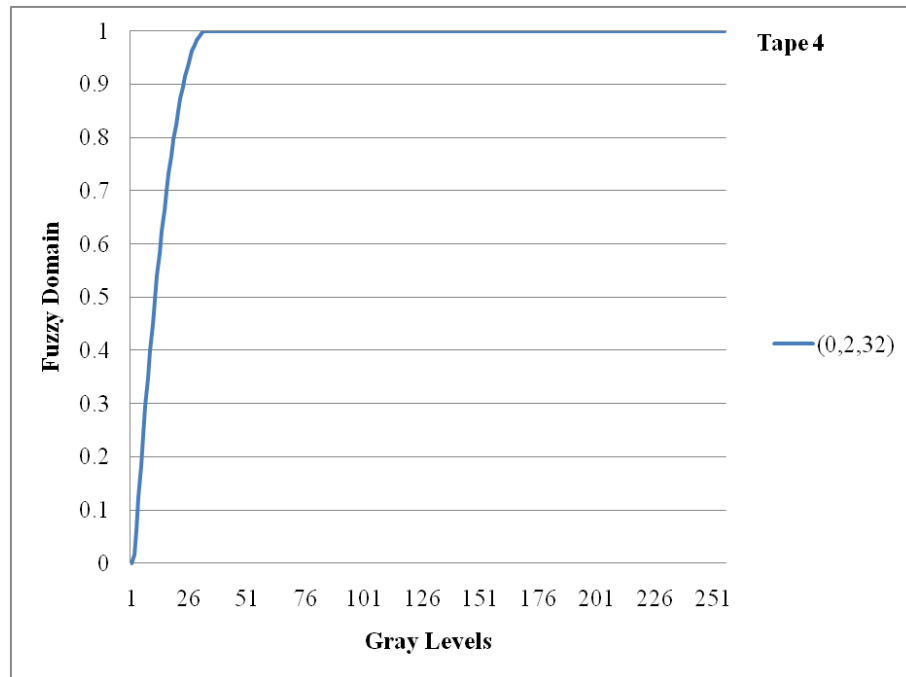


Image 4

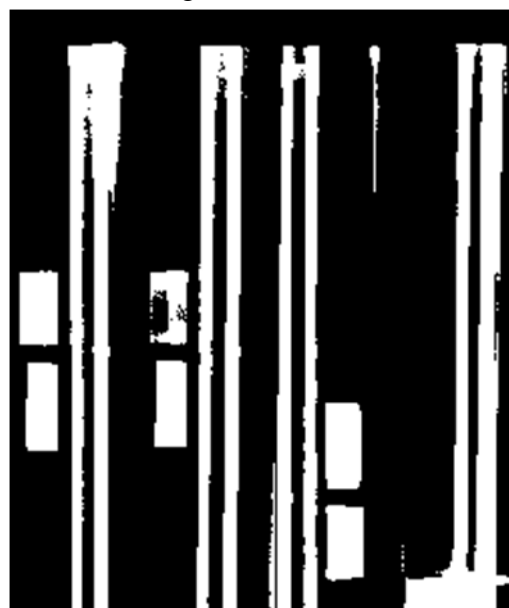
Figure 10 b The S-function plot using parameter (a, b, c) for images 3 and 4 in Table 1



(a)Image 1



(b)Image 2



(c)Image 3



(d)Image 4

Figure 11 Result of binary thresholding by Cheng et al [1], applied to sample images

5. Line Detection Using Standard Hough Transform

The Standard Hough Transform is very popular technique in image processing to find and link line segments in an image. For a given a set of points in a binary image SHT can find the subsets of those points that lie on straight lines. The figure 12 (a) helps to understand geometric interpretation of parameters ρ and θ in normal form of line given in equation (2). It shows that a horizontal line has $\theta=0$ with ρ = positive x-intercept. A vertical line has $\theta=90$ with ρ =positive y-intercept.

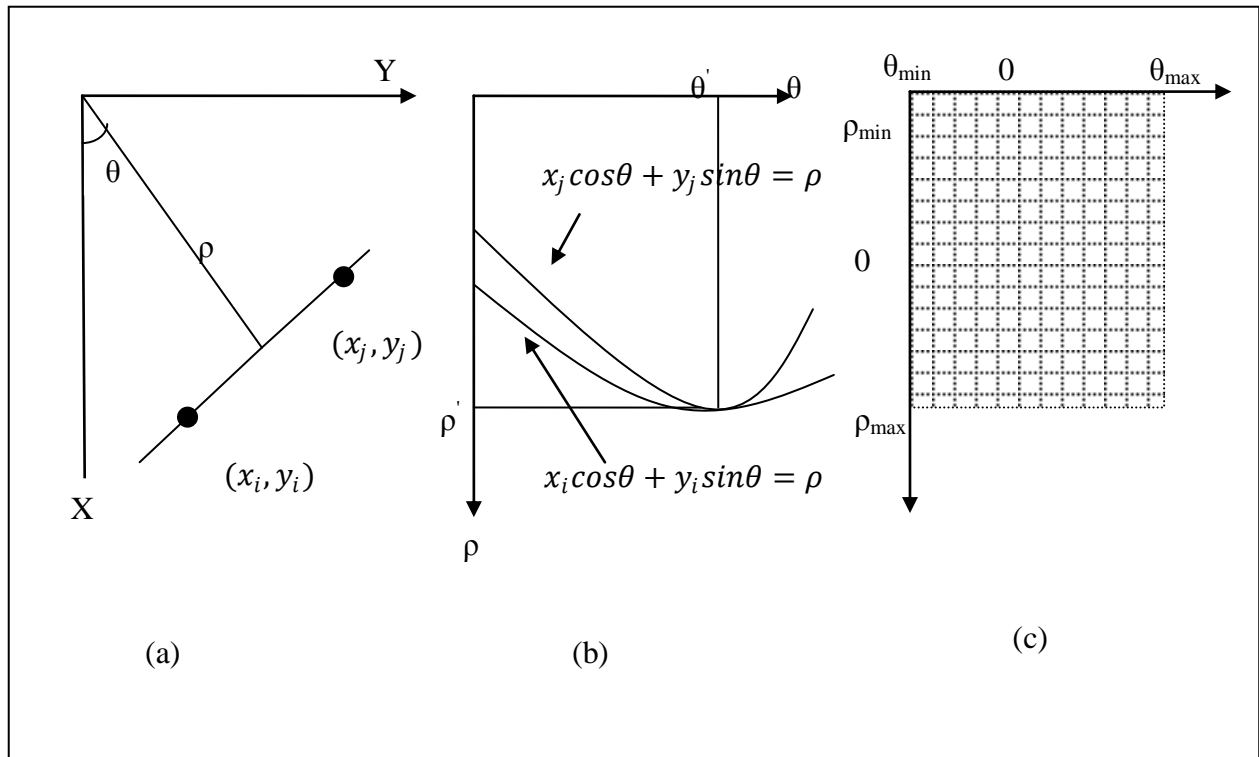


Figure 12 (a) (ρ, θ) parameterization of lines in XY-plane. (b) sinusoidal curves in $\rho\theta$ -plane; the point of intersection ρ', θ' correspond to the parameters of line joining (x_i, y_i) and (x_j, y_j) . (c) division of $\rho\theta$ -plane into accumulator cells

The figure 12 (b) shows the intersection point (ρ', θ') corresponding to the line passing through (x_i, y_i) and (x_j, y_j) . The $\rho\theta$ plane is sub-divided into accumulator cells and shown in figure 12 (c), where $(\theta_{\min}, \theta_{\max})$ and $(\rho_{\min}, \rho_{\max})$ are the expected ranges of the parameter value. Firstly, the accumulator cells are set to zero. Then for every non-zero point in the binary image, we let θ equal to each allowed subdivision value on the θ -axis and solve for ρ using equation (2). The resulting ρ - values are rounded off to nearest allowed cell value along the ρ -axis and corresponding accumulator cell is incremented. After exhausting all possible subdivisions in θ -axis the procedure is complete. At the end of the procedure, if Q is the value in cell $A(i,j)$ it means Q points lie on the line $x\cos\theta_j + y\sin\theta_j = \rho_i$. The objective is to pick the cells with maximum value from accumulator array. Finding a meaningful set of the cells with maximum values in the accumulator array is challenging. Two strategies were implemented to overcome this problem. The first strategy, threshold based method is the following (explained in detail in section 5.1):

Step 1: Find the regional maximum in Hough transform cell and record their location.

Step 2: Output only those regional maxima which are greater than specified threshold.

The second strategy, Houghpeak based method is the following (explained in detail in section 5.2):

Step 1: Find the Hough transform cell containing the highest value and record its location.

Step 2: Set to zero Hough transform cells in the neighborhood of maximum found using step 1.

Step 3: Repeat until the desired number of peaks has been found.

The Figure 11 shows the result of binarizing sample images; image 1, 2, 3, and, 4 using Cheng et al [1].

The binary image width is 250 and height is 300. Hence, D , the distance between corners in the image is 390 ($=\sqrt{250^2 + 300^2}$). In figure 6, it can be observed that lines are mostly parallel or in slight angle with X-axis in the image space. Based on this observation, the range of parameters, $(\theta_{\min}, \theta_{\max})$ and $(\rho_{\min}, \rho_{\max})$ were fixed at $(-4, 4)$ and $(1, 390)$ respectively.

In both strategies the procedure for calculating Hough transform is same. The routine for calculating Hough Transform which is common to both methods is presented below:

Step 1: Input the binary image: *Imbinary*, Initialize interval for radius of lines in polar coordinates: *pstep*, interval for angle of lines in polar coordinates: *tetastep*, threshold value: *thresh*, minimum threshold for choosing accumulator cells.

Step 2: Initialize the sub-divisions for ρ and θ of the $\rho\theta$ -plane,

$$p = 1, 1 + pstep, \dots, D, D = \sqrt{(\text{length of } Imbinary)^2 + (\text{width of } Imbinary)^2} \text{ and}$$

$$teta = (-4, -3, \dots, 4) \text{ respectively, } tetastep = 1.$$

Step 3: Initialize an accumulator array with zeros: *Accumulator*, where number of rows = length of p , number of columns = length of *teta*.

Step 4: Find location of non-zero pixels, *xIndex*, *yIndex*, Points (x, y) in *Imbinary* = 1

Step 5: FOR Counter = 1 to End (*xIndex*)

Index of angle in accumulator array, $Indteta = 0$

FOR $tetai = -4$ to $4 * \pi / 180$

i. $Indteta = Indteta + 1$

ii. Solve radius for each angle, $tetai$ using equation (2)

iii. $R = xIndex(cnt) \times \cos(tetai) + yIndex(cnt) \times \sin(tetai)$

IF $1 \geq R \geq \text{upper bound of } p$ **THEN**

i. Find location of p , closest matching with R , $Indp$

ii. Increment accumulator cell,

$Accumulator(Indp, Indteta) = Accumulator(Indp, Indteta) + 1$

END IF

END FOR

END FOR

5.1 Finding line coordinates using SHT algorithm- Threshold based method

To explore the line detection using SHT algorithm – Threshold based method; we use a computer program available on the open exchange forum for Matlab users called Matlab Central [22]. The computer program uses Standard Hough Transform – threshold based method to detect lines in binary image. The procedure for binarization of image is already explained in detail in Chapter 5. After completing the routine for determining Hough transform on binary image, the following steps are followed:

Step 1: Calculate regional maxima in accumulator array,

$$Accumulatorbinarymax = \textbf{IMREGIONALMAX}(Accumulator)$$

Step 2: Find location of regional maxima in *Accumulatorbinarymax*,

$$(Potential_p, Potential_teta) = \text{where } Accumulatorbinarymax == 1$$

Step 3: If value of regional maxima in original accumulator array is greater than threshold, *thresh*, include in output,

$$\textbf{IF } Accumulator(Potential_p, Potential_teta) - thresh \geq 0 \textbf{ THEN}$$

$$final_p = Potential_p, final_teta = potential_teta$$

Step 4: Output the result, *final_p* and *final_teta*

The accumulator array can be thought of in three dimensions: the θ - and ρ -axes represent line positions and the z-axis represents number of collinear points in each line. The cells with high intensity and low intensity can be important because they often represent relevant objects. We are only interested in finding cells with high intensity. The **IMREGIONALMAX** Matlab function is used to find regional maxima. A regional maximum is true where 8 connected components all have same value, and whose external boundary pixels all have lower value.

In summary, the Standard Hough Transform algorithm-threshold based method can be used to find the polar coordinates i.e., radius and angle of lines in the binary image. Major parameters associated with SHT algorithm-threshold based include interval for radius of line, *pstep*, interval for angle, *tetastep*, threshold, *thresh*. For this study, they are fixed at 1, 1 and 100 respectively.

The result of SHT algorithm – threshold based line detection for sample images; image 1, 2, 3, and 4 is given in Table 2. The lines detected using SHT algorithm- threshold based method is

grouped into 4, 5 and 6 and 10 lines using cluster technique. The cluster technique is explained in Chapter 6.

Table 2 Result of SHT algorithm-Threshold based method for sample images

Image 1	ρ	22	139	202	27	145	207	32	83	85	132	213	90
	θ	-4	-4	-4	-3	-3	-3	-2	-2	-2	-2	-2	-1
	ρ	153	154	204	54	94	142	154	155	156	157	158	159
	θ	-1	-1	-1	0	0	0	0	0	0	0	0	0
	ρ	206	219	220	221	41	97	98	144	157	158	159	160
	θ	0	0	0	0	1	1	1	1	1	1	1	1
	ρ	208	223	224	225	100	102	148	227	49	50	104	152
	θ	1	1	1	1	2	2	2	2	3	3	3	3
	ρ	166	231	56	170								
	θ	3	3	4	4								
Image 2	ρ	9	73	146	210	222	225	13	75	77	80	106	149
	θ	-4	-4	-4	-4	-4	-4	-3	-3	-3	-3	-3	-3
	ρ	215	3	5	20	67	85	111	156	221	236	24	72
	θ	-3	-2	-2	-2	-2	-2	-2	-2	-2	-2	-1	-1
	ρ	115	140	226	241	11	12	13	28	29	76	77	145
	θ	-1	-1	-1	-1	0	0	0	0	0	0	0	0
	ρ	161	162	163	164	226	227	228	229	243	245	13	14
	θ	0	0	0	0	0	0	0	0	0	0	1	1
	ρ	15	29	30	31	32	78	79	80	81	148	163	164
	θ	1	1	1	1	1	1	1	1	1	1	1	1
	ρ	165	166	229	230	231	245	247	96	166	250	23	37

	θ	1	1	1	1	1	1	1	2	2	2	3	3
	ρ	87	239	30	42	93	107	163	176	182	247		
	θ	3	3	4	4	4	4	4	4	4	4		
Image 3	ρ	29	93	132	133	217	221	33	97	136	138	147	224
	θ	-4	-4	-4	-4	-4	-4	-3	-3	-3	-3	-3	-3
	ρ	39	89	102	130	143	219	232	30	31	42	43	44
	θ	-2	-2	-2	-2	-2	-2	-2	-1	-1	-1	-1	-1
	ρ	108	32	33	34	35	36	43	44	45	46	47	48
	θ	-1	0	0	0	0	0	0	0	0	0	0	0
	ρ	49	96	97	98	109	110	111	112	113	137	138	139
	θ	0	0	0	0	0	0	0	0	0	0	0	0
	ρ	140	149	150	151	152	224	225	226	227	37	48	49
	θ	0	0	0	0	0	0	0	0	0	1	1	1
	ρ	50	51	100	101	102	112	113	114	115	139	140	141
	θ	1	1	1	1	1	1	1	1	1	1	1	1
	ρ	153	154	227	228	229	230	53	104	231	242	48	57
	θ	1	1	1	1	1	1	2	2	2	2	3	3
	ρ	109	121	162	185	62	115	127	155	240	254		
	θ	3	3	3	3	4	4	4	4	4	4		
Image 4	ρ	10	12	90	99	136	150	162	210	223	224	225	228
	θ	-4	-4	-4	-4	-4	-4	-4	-4	-4	-4	-4	-4
	ρ	2	16	20	93	138	155	216	233	235	6	23	24
	θ	-3	-3	-3	-3	-3	-3	-3	-3	-3	-2	-2	-2
	ρ	138	144	159	221	8	11	28	71	100	101	102	103

	θ	-2	-2	-2	-2	-1	-1	-1	-1	-1	-1	-1	-1
	ρ	147	176	177	178	179	180	224	225	241	13	28	29
	θ	-1	-1	-1	-1	-1	-1	-1	-1	-1	0	0	0
	ρ	30	31	32	33	73	102	103	104	105	106	117	179
	θ	0	0	0	0	0	0	0	0	0	0	0	0
	ρ	180	181	225	226	227	228	229	230	244	245	16	18
	θ	0	0	0	0	0	0	0	0	0	0	1	1
	ρ	32	33	34	35	75	107	156	170	229	230	12	21
	θ	1	1	1	1	1	1	1	1	1	1	2	2
	ρ	111	112	174	188	24	26	40	117	163	177	193	194
	θ	2	2	2	2	3	3	3	3	3	3	3	3
	ρ	237	256	31	45	120	123	166	200	245	259		
	θ	3	3	4	4	4	4	4	4	4	4		

5.2 Finding line coordinates using SHT algorithm- Hough Peak based method

The same problem of choosing a set of cells with maximum value in accumulator array can be solved using Houghpeak based method. Firstly, '*Hough*' function available in image processing toolbox in Matlab software was used to determine Hough transform. The range of parameters, $(\theta_{\min}, \theta_{\max})$ and $(\rho_{\min}, \rho_{\max})$ were fixed at $(-90, 89)$ and $(1, 390)$ respectively. Essentially, it was made sure that Hough transform is first generated. Then, '*Houghpeaks*' function available in image processing toolbox in Matlab software was used to find exactly 4, 5 and 6 and 10 peaks. The *Houghpeaks* function is presented below:

$Peaks = Houghpeaks (Accumulator, maxpeak, adaptivethresh)$

Step 1: Initialize *done* = FALSE, variable to end loop; *adaptivethresh*, minimum adaptive threshold; *nhoodsize*, neighborhood around peak cell that is set to zero after peak cell identified; *numpeaks*, number of peaks; *maxpeak*, maximum number of peak cells to be found.

Step2: Find location of global maximum in Accumulator array,

$(Potential_p, Potential_teta) = MAX(Accumulatorbinarymax)$

Step 3: If global maximum $\geq adaptivethresh$,

Append *Potential_p*, *Potential_teta* to output, *final_p* and *final_teta*

If all peaks are found, *numpeaks*=*maxpeak*; Go to step 5

Else continue to step 4

If global maximum $< adaptivethresh$

Go to step 5

Step 4: Suppress global maximum cell and neighbor cells,

global maximum cell to global maximum+ *nhoodsize* = 0; After updating *Accumulator* go to step 2.

Step 5: *done*=TRUE; Output *final_p* and *final_teta*. END

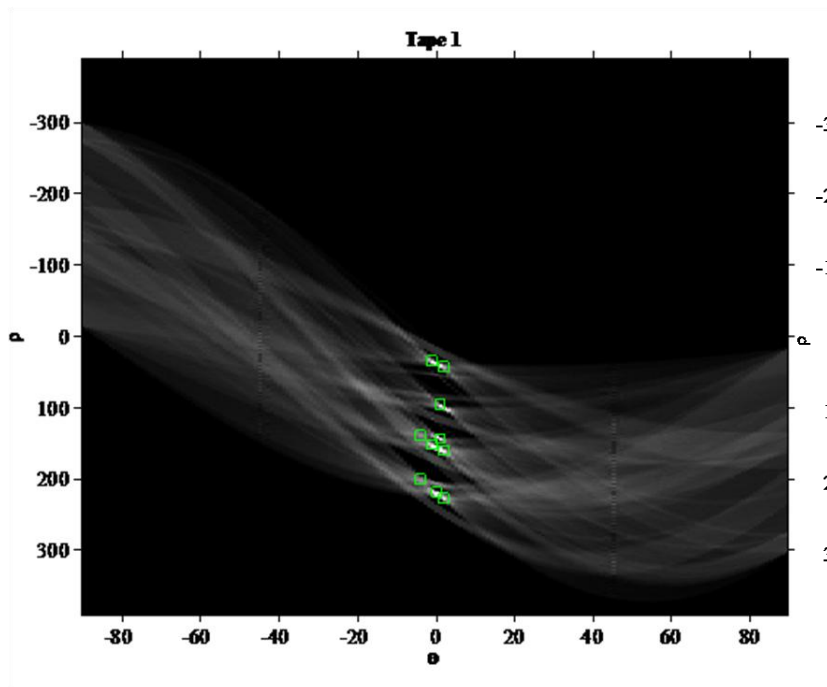
The *Houghpeaks* function basically finds a set of peaks in the Hough transform. The major input parameters include *maxpeak*, maximum number of peaks to identify; *adaptivethresh*, the adaptive threshold and *nhoodsize*, the neighborhood around each peak cell that is set to zero after peak is identified. The maximum number of peak cells found was 4, 5 and 6 and 10. The

adaptive threshold was calculated using the formulae $0.3 \times (\text{Global Maximum of Accumulator})$. Parameter $nhoodsize$ was fixed at 17 along ρ sub-division and 3 along the θ sub-division of the accumulator array. In summary, Houghpeak based method is different from threshold based method in the following areas. First of all it is iterative in nature and finds a fixed number of peak cells. Secondly, the minimum threshold is adaptive to the Hough transform. The result of Houghpeak based method of binary image 1 is shown in Table 3. Figure 13, summarizes the position of 10 peaks found in Hough transform of sample images.

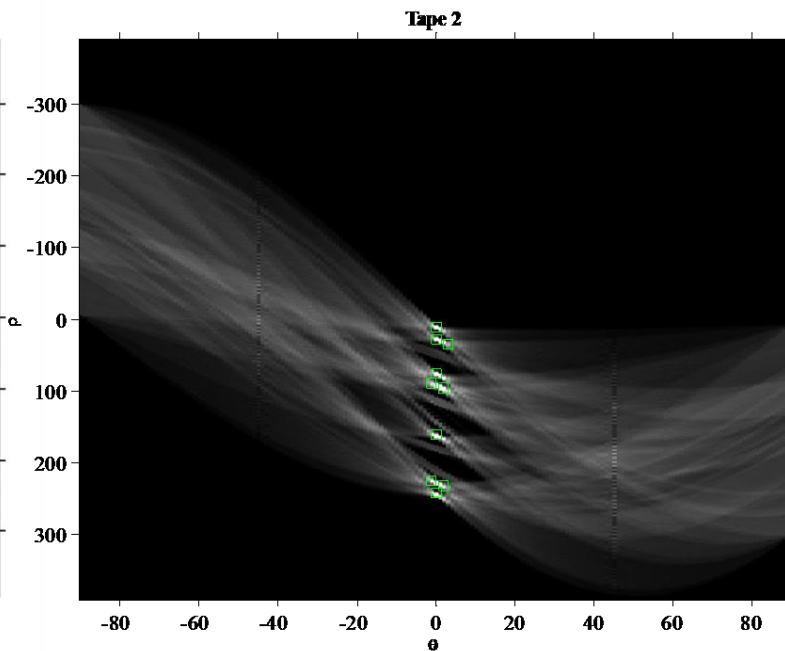
Table 3 Output of SHT algorithm- Houghpeak based method of sample images.

Image 1	10 peaks	ρ	218	34	152	96	160	143	227	43	201	138
		θ	0	-1	-1	1	2	1	2	2	-4	-4
Image 2	10 peaks	ρ	225	10	27	96	75	160	242	89	232	34
		θ	-1	0	0	2	0	0	0	-1	2	3
Image 3	10 peaks	ρ	237	41	107	223	50	30	95	136	148	246
		θ	1	-1	-1	0	1	-1	0	0	0	3
Image 4	10 peaks	ρ	223	170	160	179	99	27	243	35	12	152
		θ	-1	1	-1	-1	-1	-1	0	2	0	-4

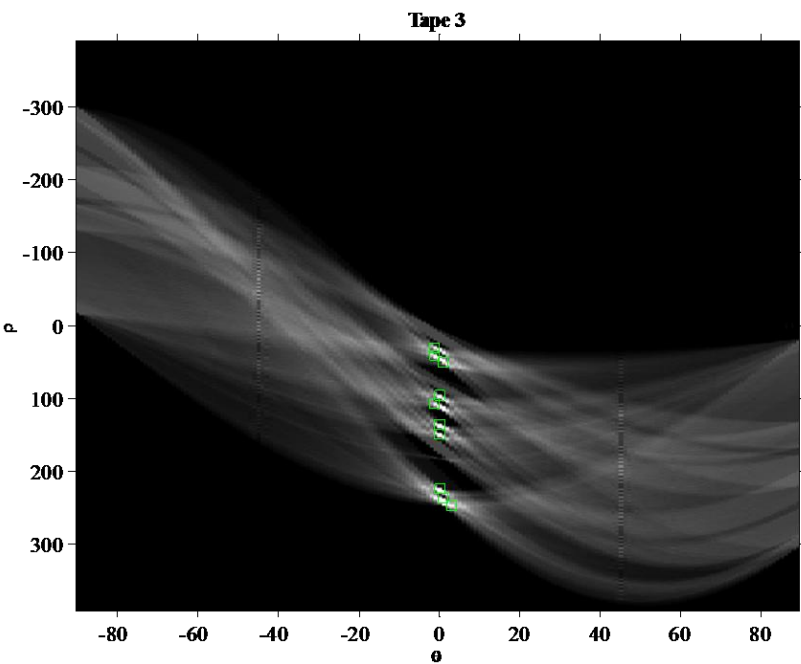
It is observed that, the lines suppressed during iteration are weld. Also the lines detected by this method are able to detect non-welds. We propose a post-processing procedure in Chapter 7. The post-processing is final step in this research. Thus in this section, lines were detected using SHT algorithm-Houghpeak based method for the sample images.



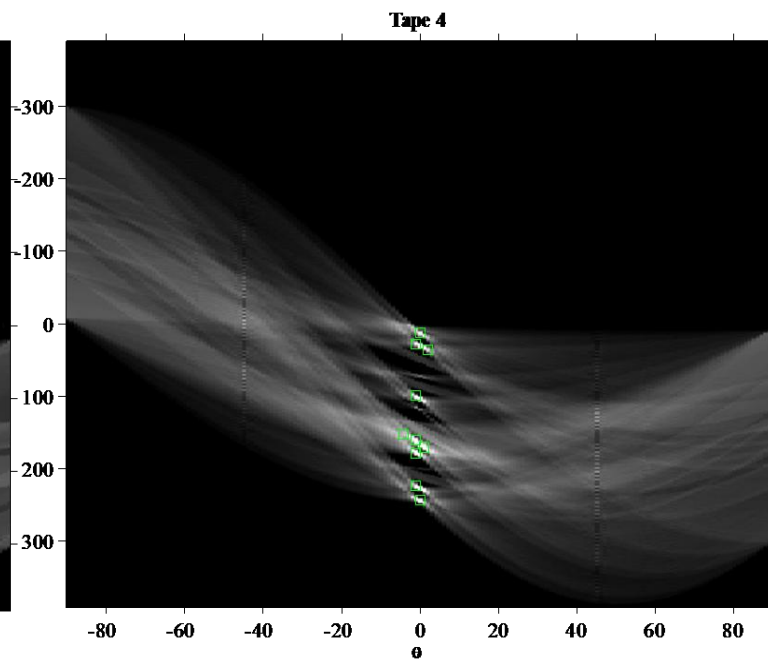
(a)Image 1



(b) Image 2



(c)Image 3



(d) Image 4

Figure 13 Position of 10 peaks in the Hough transform matrix of sample images

6. Fuzzy C-means For Clustering Lines Detected Using SHT Algorithm- Threshold Based Method

The Fuzzy C-Means (FCM) algorithm is used to cluster lines detected by SHT algorithm-threshold based method. The result of threshold based methods cannot be used directly to find welds because it finds a huge number of lines. The number of lines has to be lowered by a meaningful procedure so the weld lines remain while non-weld lines are removed. Fuzzy C-means is a popular fuzzy clustering method that is algorithmic in nature used to find clusters in a given set of data. The main objective of is to partition a collection of data into clusters whose degree of belongingness is understood as membership value. Consider, n vectors $x_1, x_2, x_3, \dots, x_n$ equipped with a distance between two elements x_i and x_j , denoted by $\|x_i - x_j\|$. The objective of clustering is such that objects within a cluster are similar and between the clusters are dissimilar.

The objective function can be written as non-linear optimization problem:

$$\text{Minimize: } \sum_{i=1}^c \sum_{k=1}^n U_{ik} \|x_k - v_i\|^2 \quad (12)$$

$$\text{Subject to: } U_{ik} \in \{0,1\} \forall i, k$$

$$\sum_{i=1}^c U_{ik} = 1 \forall k$$

$$0 < \sum_{k=1}^n U_{ik} < n \forall i$$

where x_k is an object, $k=1, 2, 3 \dots n$ objects, v_i is cluster center, $i=1, 2, 3, \dots, c$ clusters, U_{ik} , is the membership degree of object x_k in cluster i .

The ‘FCM’ function available in Matlab was used to solve the above given optimization problem. The *FCM* function is available part of fuzzy logic toolbox in Matlab software.

The pseudo code of *FCM* function is given below:

Step 1: Initialize by random generation *V*

Do while counter \leq MAX_ITR, maximum number of iterations

$$\text{Step 2: Compute } U, U_{ik} = \frac{1}{\sum_{j=1}^c \left(\frac{\|x_k - v_i\|}{\|x_k - v_j\|} \right)^2} \quad \forall i, k$$

$$\text{Step 3: Update } V, V_i = \frac{\sum_{k=1}^n U_{ik}^2 x_k}{\sum_{k=1}^n U_{ik}^2}$$

Step 4: If change in *V* $< \epsilon$, where ϵ is a very small number STOP and go to step 6.

Step 5: Increment counter by 1 each time.

End while

Step 6: Get the final output *U* and *V*.

The major parameters associated with FCM function are: *c*, number of clusters; ϵ the stopping criteria for the algorithm; MAX_ITR, maximum number of iteration. The number of clusters found was 4, 5, 6 and 10. The value of parameters ϵ and MAX_ITR were fixed at 10^{-5} and 100 respectively.

The lines detected using threshold method for image 1 was grouped, for *c*=10, the cluster centers found using FCM algorithm was: 27, 168, 144, 134, 157, 51, 206, 86, 100, and 224. The number of objects identified in each cluster was: 3, 2, 4, 2, 13, 5, 6, 3, 6, and 8 respectively. Figure 14 shows the clustering using the fuzzy toolbox available in Matlab software.

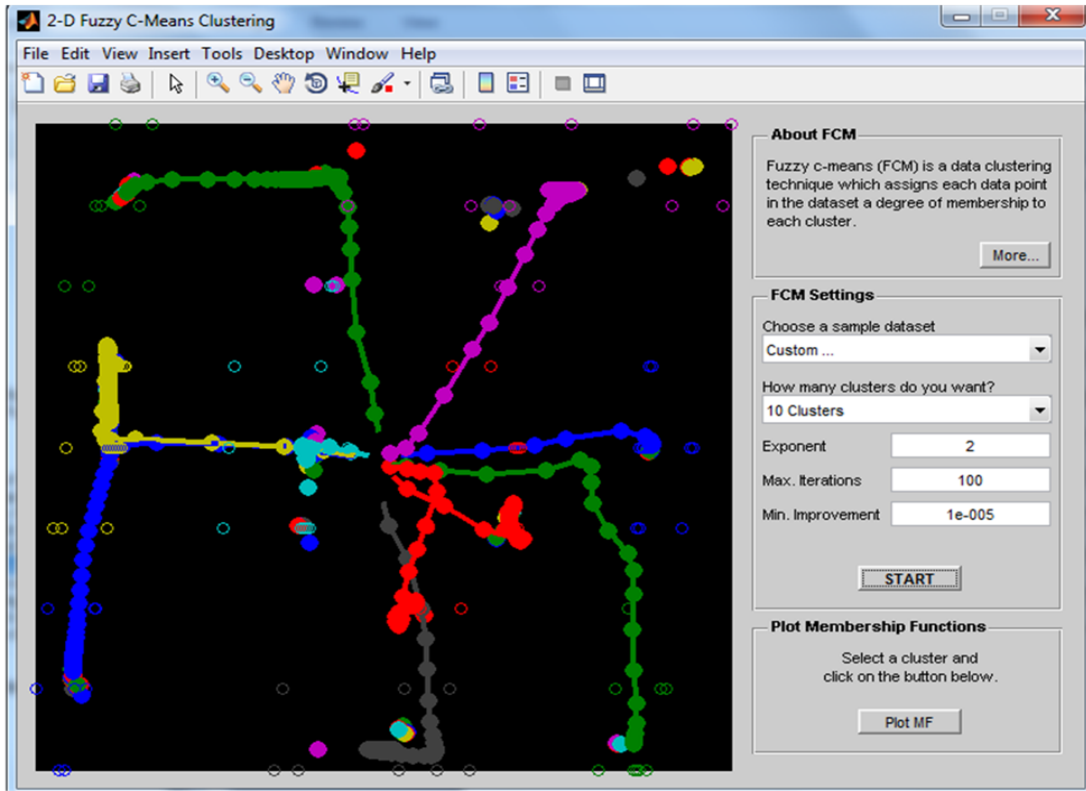


Figure 14 Clustering of objects in the ρ , θ vector using FCM toolbox of Matlab software

In this section, the lines detected using SHT algorithm-threshold based method is grouped using FCM method. The summary of results is presented in Table 4.

Table 4 Result of Clustering at $C=10$ for sample images.

Image 1	10 C	ρ	27	168	144	134	157	51	206	86	100	224
		θ	-3	3	0	-2	0	2	-1	-2	2	1
Image 2	10 C	ρ	91	146	76	163	12	30	180	110	244	226
		θ	2	-1	-1	1	-1	1	4	-1	1	-1
Image 3	10 C	ρ	95	48	102	34	185	152	113	226	138	244
		θ	-2	1	1	-1	3	1	1	-1	-1	3
Image 4	10 C	ρ	93	226	31	121	246	12	154	180	104	73
		θ	-3	-1	1	2	2	-1	-2	0	0	0

7. Post-Processing To Find Lines That Are Weld

The image contains several reference objects like rulers, penetrometers, densitometers, identification letters, and space between weld strips. Some of these objects (non-welds) are very similar to weld in terms of their length and intensity. These objects are not of interest to the weld inspection system. Only the objects inside the weld are of interest [3]. Post-processing is the final step in this research to separate linear welds from background and non-weld. Ideally, location of line found using standard Hough transform algorithm should correspond to the location of weld only. The parameters *thresh* in SHT algorithm, as described in chapter 5, is set to 100 to capture the weld as it is known that minimum length of weld is definitely more than 100. However the lines detected using SHT algorithm are able to detect some non-welds. Also, the lines detected using SHT algorithm –Houghpeaks based method are able to detect some non-welds. Although it is not possible to eliminate all non-welds, this step can overcome the problem of false detection and increase the true detection of weld, post-processing is very necessary. Therefore, post-processing is used to classify lines that are weld. The result of SHT algorithm, 10 lines detected using SHT algorithm- threshold and Houghpeak based method are identified as weld.

This chapter presents the approach of post-processing operation used in this research. Firstly a portion of the original image containing the weld is extracted based on lines detected using Hough Transform. Secondly, weld-peak detection method is applied. The weld-peak detection is explained in Section 7.1.

The information contained in the extracted portion, as the result of the first step, are the pixel intensities of the objects, both weld and non-weld. The weld object has its pixel intensity distribution very similar to a Gaussian curve [3]. Also based on their observation it can be said that non-weld objects do not have a Gaussian like distribution. This creates an opportunity to

identify the objects having one or more peak as a weld and objects without any peak or with flat peaks as non-weld. In case of weld objects the location of first peak is considered to be the location of weld.

Liao and Ni [3] had divided the original image into four equal parts and applied a peak/trough detection algorithm to each part for finding the peak and trough in each portion. Using the peak and trough location in the image, several features of weld are extracted, and eventually the weld location. In this research, we carry out the following post-processing procedure to find weld location:

Step 1: Find the location of line detected using SHT algorithm, $line_loc$.

Step 2: Extract sub-images for each line, using the Image extraction procedure.

Image extraction procedure:

Center of sub-image = $line_loc$

Left of sub-image = $line_loc - 10$

Right of sub-image = $line_loc + 10$

IF left of sub-image < left corner of original image OR right of sub-image > right corner of original image THEN; Left of sub-image = 0 and Right of sub-image = 250

Step 3: Extract line image corresponding to $X=50$ for each sub-image. The line image can be extracted at any point along the x-axis of the sub-image.

Step 4: Detect objects in each line image by applying weld-peak detection algorithm, to be presented in chapter 7.1.

Step 5: IF a Peak is detected THEN; sub-image contains weld and Weld location = Peak location of object.

7.1 Weld-peak detection for detecting weld location

Liao and Ni [3] had observed the intensity plot of a line image. Based on their observation, the intensity plot of weld object looks more like Gaussian than other objects in the image. The intensity plot of a line image is taken to see the difference between weld and non-weld objects. For the purpose of this research we had applied the peak (trough) detection algorithm proposed by Liao and Ni [3]. A slight modification was made to that algorithm and is called as weld-peak detection algorithm. The weld-peaks are detected by looking for sign changes in the slope of line image. The number of weld-peaks detected is determined by the window size. Window size is the number of steps on both sides of a point that must be monotonically increasing or decreasing so the point can be called a weld-peak. The window size is determined as three, which is small enough to identify the weld's peak. If a flat peak was found it is treated as non-weld and the peak was ignored. The way flat peaks are dealt in the algorithm is the key difference between weld-peak detection algorithm and the method suggested in [3]. The center of sub-image, line_loc is chosen from output of SHT algorithm (using two methods). Either of the two methods can be used but we have tried both methods. The output SHT algorithm, i.e. 10 lines was inspected for weld using weld-peak detection algorithm. Once a peak was identified the location of peak is concluded as location of weld. An intensity plot of line image taken from the sub-image-1 of image 1, center = 218, left = 208, right = 228 and X=50 is shown in Figure 15. This center, left

and right of the intensity plot correspond to first line's location found using Houghpeak based method, for binary image 1.

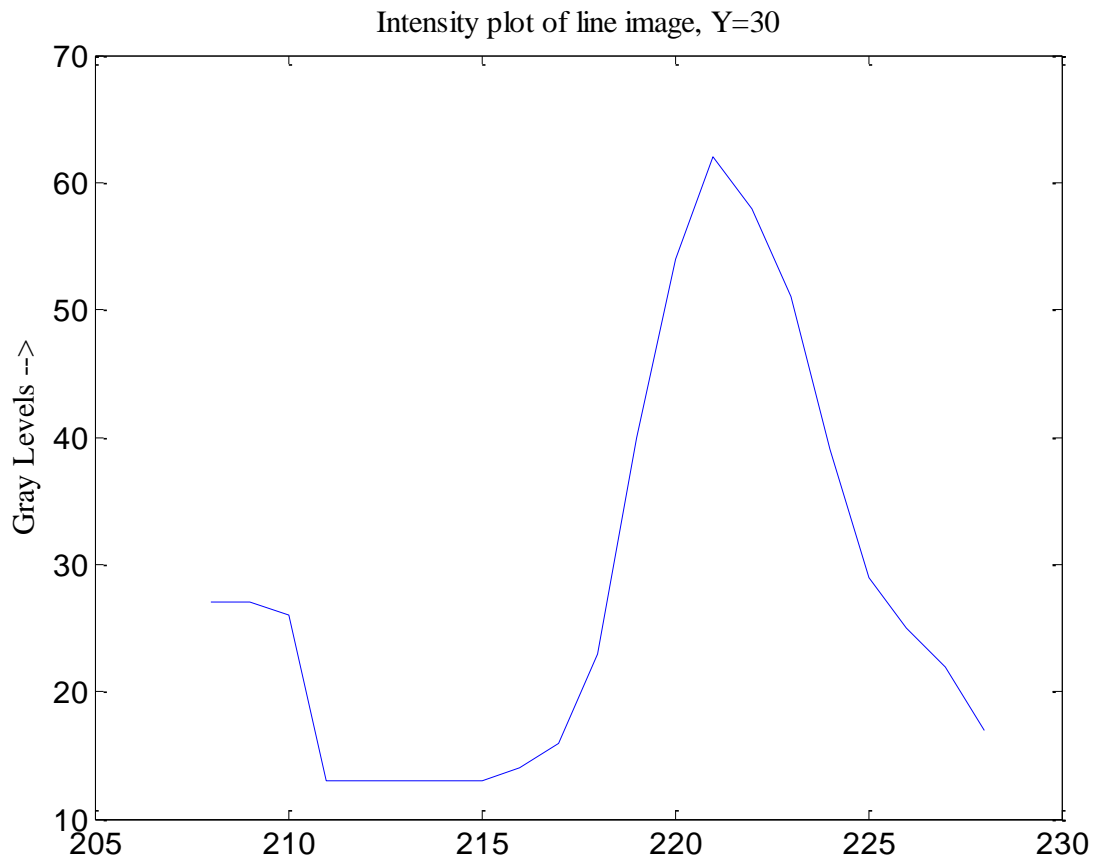


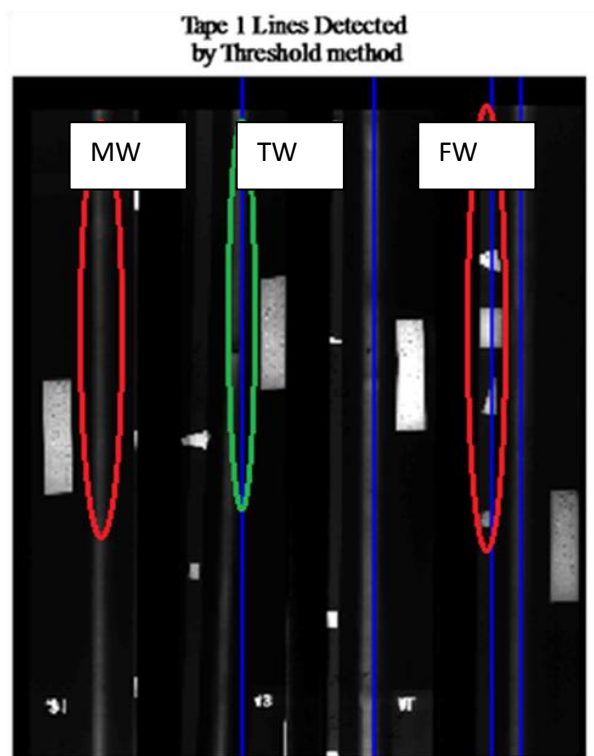
Figure 15 Intensity plot of line image at X=50, center = 218, left =208 and right= 228 of image 1

The peak determined by weld-peak algorithm for sub-image 1 of image 1 is at Y=222 (Y intercept). The final welds were located at y=38, y=100, y=158, y=209 and y=222. Based on visual examination, four welds were found to be true and one was a false alarm. A line at y=209 is non-correctly identified as weld. The criterion for accepting detection result is that, if a straight line is drawn starting at x=0 and y=weld-peak location, it should be lying within the weld thickness. Another example, the two lines determined using threshold method for binary image 1

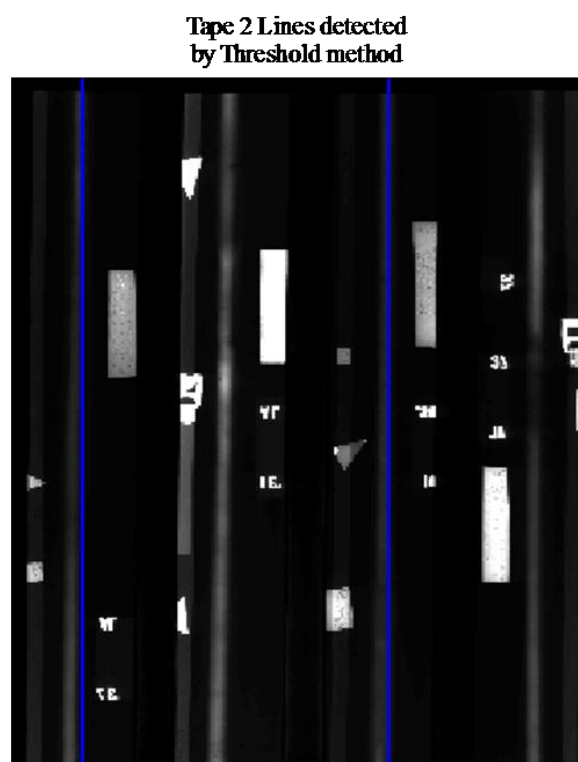
are 27 and 41. Their corresponding sub-images are missing the weld region which is located at $y=38$. So, the final three welds were located at $y=100$, $y=158$ and $y=222$. The lines found by threshold method located at $y=27$ and $y=41$ were determined by weld-peak algorithm as non-weld locations. Based on visual examination this was found to be true. Figure 16 summarizes the welds detected by threshold based method for sample images; image 1, 2, 3, and 54. Figure 17 summarizes the welds detected by Houghpeaks based method for sample images; image 1, 2, 3, and 4.

Table 5 summarizes the result of weld-peak detection of both Houghpeak and threshold based methods using 10 lines. Both methods were tested using 25 images; there are 4 welds per image, total of 100 actual welds. The Houghpeak based method was found to detect 87 True Weld (TW). The true welds detected by threshold based method are 81. There is no significant difference between two methods in true detection of welds. The number of False Weld (FW) detected by Houghpeak is lower than threshold based method at 31. A false weld is actually not weld but detected by the method as weld. Similarly a Missed Weld (MW) is actually weld but detected by method as non-weld. Missed welds by Houghpeak method is also lower than threshold method at 13.

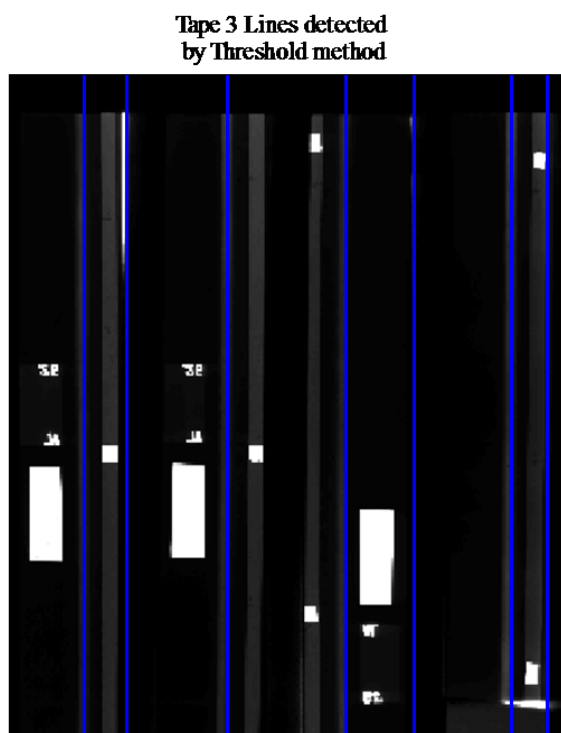
We observed that choosing more number of lines will yield more true detections. However, increasing the number of lines will also increase the number of false welds, thus decreasing the accuracy of detection. For threshold method, picking 4, 5, and 6 lines gave 59, 64, and 70 TW and 3, 13, and 17 FW. For Houghpeak method, picking 4, 5, and 6 lines yielded 59, 71, and 78 TW's and 9, 13, and 20 FW.



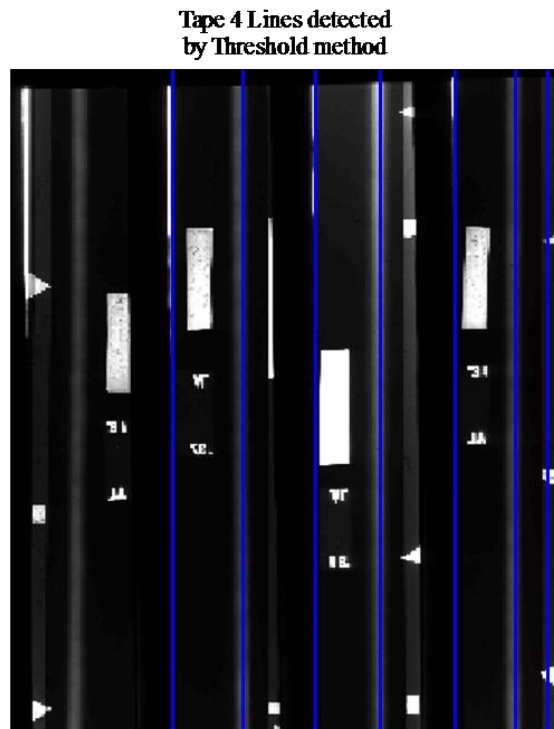
(a)Image 1



(b)Image 2



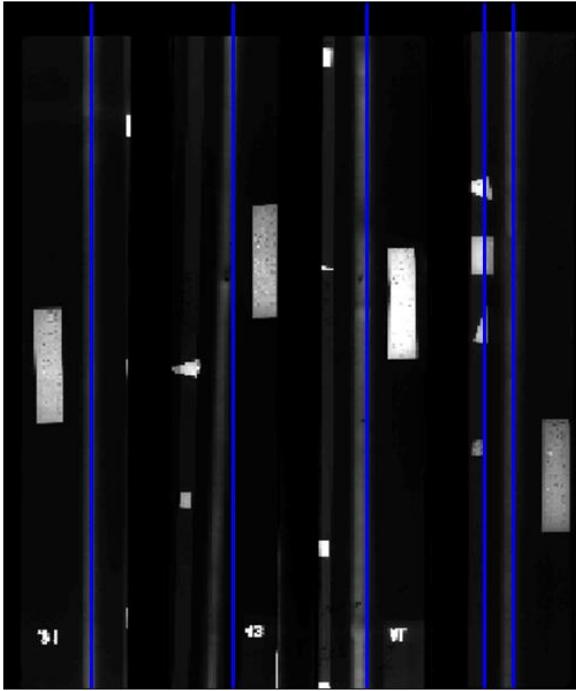
(c)Image 3



(d)Image 4

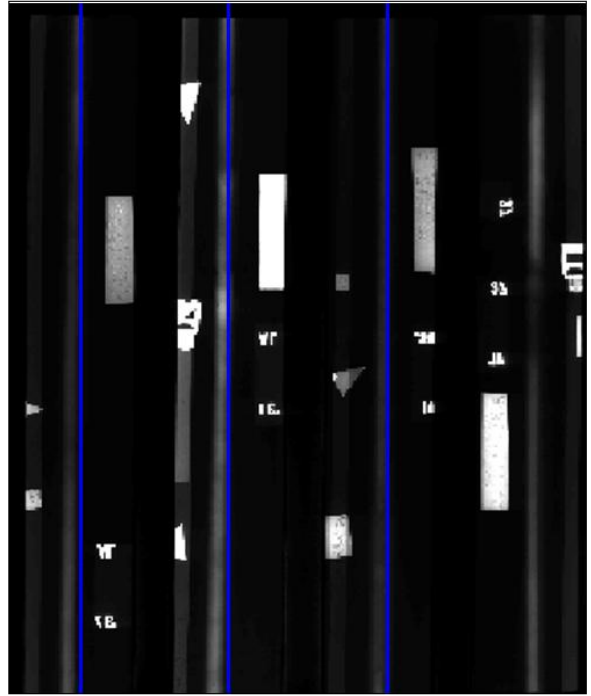
Figure 16 Summary of results of Threshold based method (a) Welds in image 1; (b) Welds in image 2; (c) Welds in image 3; (d) Welds in image 4

Tape 1 Lines detected by Houghpeak method



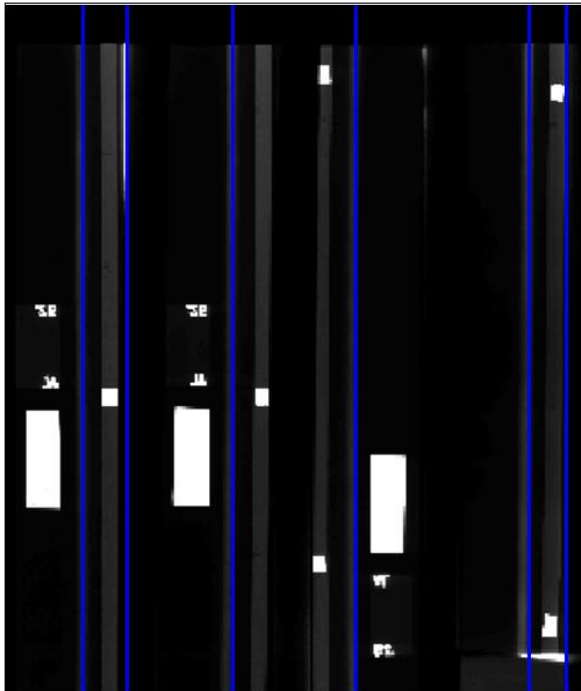
(a)Image 1

Tape 2 Lines detected by Houghpeak method



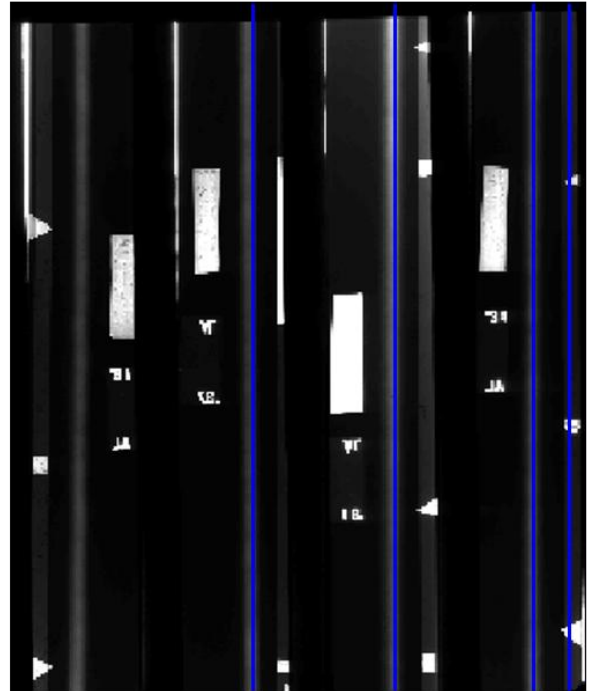
(b)Image 2

Tape 3 Lines detected by Houghpeaks method



(c)Image 3

Tape 4 Lines detected by Houghpeak method



(d) Image 4

Figure 17 Summary of results of Houghpeaks based method (a) Welds in image 1; (b) Welds in image 2; (c) Welds in image 3; (d) Welds in image 4

Table 5 Result of Threshold and Houghpeak based methods. Confusion matrix for 100 actual welds using 25 test images

Predicted			Actual	
	By SHT algorithm-Houghpeak based method		Weld	Non-weld
		Weld	87	31
		Non-weld	13	119
	By SHT algorithm Threshold based method	Weld	81	44
		Non-weld	19	106

7.2 Effects of changing ρ -axis cells in *Accumulator* array

In SHT algorithm- Houghpeak based method, the sub-divisions for ρ θ parameter in accumulator array was fixed at 1 and the ranges were fixed at (1, 390) and (-90 89) respectively. The Hough transform generated is obviously dependent on the allowed sub-divisions it can take on the ρ -axis. Allowing more cells in accumulator array along ρ -axis will yield higher accuracy of line detection. Also, allowing lesser cells in accumulator array along ρ -axis is expected to yield poor line detection. To see the change in lines detected, SHT algorithm-Houghpeak based method is used to detect 10 lines. In order to verify the welds detected weld-peak detection algorithm has been used. The values of sub-divisions on ρ -axis were changed to: 0.5, 5, and 10. Corresponding parameter *nhoodsize* along ρ sub-division was also changed to: 33, 5 and 3 respectively. The

lines detected using SHT algorithm-Houghpeak based method was classified as weld using weld-peak detection algorithm. Table 6 summarizes the welds detected by changing the parameter sub-division on ρ -axis.

Table 6 Confusion matrix for 100 actual welds at different ρ sub-divisions

Predicted			Actual 100 weld	
	At ρ sub-division = 0.5		Weld	Non-weld
		Weld	88	40
		Non-weld	12	110
	At ρ sub-division = 5	Weld	85	30
		Non-weld	15	120
	At ρ sub-division = 10	Weld	74	24
		Non-weld	26	126

It can be observed in Table 6 that true welds detected are higher when the ρ -axis cells in accumulator array are increased.

7.3 Effects of changing the adaptive threshold in Houghpeak based method

In the Houghpeak based method, we set the value for adaptive threshold, *adaptivethresh* equal to $0.3 \times (\text{Global maximum of Accumulator})$. This parameter played major role in iteration to disqualify peaks which were below certain threshold. The threshold was obviously adaptive to the Accumulator array of the image. To see the effects of this parameter to line detection, we

changed the value of this parameter to $0.2\times$, $0.4\times$ and $0.5\times$ (global maximum of *Accumulator*). We observed the change in the line detection because of this parameter by keeping other parameters at their fixed values. The number of lines detected and welds detected remain same for each values of parameter, *adaptivethresh*.

8. Conclusion and Discussion of Results

The main goal of this research was to explore the possibility of using line detection method to detect linear welds. We did a detailed study of applying Standard Hough Transform algorithm to weld extraction. Automatic weld extraction using SHT algorithm was realized in 3 major steps. Firstly, an optimization model was developed to replicate the method by Cheng et al [1] for binarization of image using Matlab software. The optimization model is used for finding single threshold intensity level. We have used single threshold for binarization of gray scale image. Further studies could involve experimentally determining the best thresholding technique for binarization of grayscale image. We had observed that for a few sample images the welds were also removed along with other non-weld objects. It is because these images have very low contrast and very poor illumination near the welds. So, preprocessing steps could be used, such as histogram equalization, to enhance the contrast in poor images.

The optimization problem is solved using simulated annealing algorithm by Bohachevsky et al [9]. The optimization model solved by simulated annealing method was replicated using Matlab software. Based on the optimization results, the following observations were made:

1. The SA algorithm is probabilistic in nature. The optimal solution found in each run varies so 20 runs were done and the best solution of 20 runs was selected.
2. Since the gray-level of some welds are overlapping with the gray-level of the gaps between two films strips, it is very difficult to choose a threshold value that will separate weld and non-weld. Hence, it is not possible to retain the welds in all binarized images.

Secondly, the SHT algorithm was used to transform the binarized image to Hough transform. After calculating the Hough transform, two different approaches were followed to select peak

cells in the Hough transform. In our first approach, we adopted a fixed threshold and found the regional maxima cells. The parameter *thresh* plays a significant role in SHT algorithm-threshold based method. This parameter *thresh* was set as 100 for this study. It should be large enough to avoid non-weld objects and small enough to include all weld objects.

In our second approach, we adopted an iterative procedure called Houghpeak based method to find fixed set of peak cells using adaptive threshold. Finally, a post-processing method was also developed to find lines that are weld. The post-processing method was based on the observation that weld-objects resemble Gaussian [3]. The SHT algorithm-threshold and Houghpeak based methods, detect 6 lines that are finally used to find welds. The one with lower false alarm rate could also be chosen for finding weld lines using weld-peak detection method. The weld-peak detection is introduced in this thesis which is different from peak detection [3] in the way it treat flat peaks. We changed the ρ -axis cells in accumulator array to see its effects on the weld lines detected. Increasing the allowed sub-divisions of ρ cells in accumulator array is desired for higher accuracy of line detection and higher accuracy of weld detection.

For future work, experimental investigations need to be carried out to verify the effect of contrast enhancement of the image before the thresholding step. The thresholding step has been explained in detail in this thesis. A contrast enhancement can be preceded before thresholding to see the effects in binarization of image. The effect of input variables for SHT algorithm-threshold based method: *thresh*, ρ , and θ cells can be changed to see their effect on the results. Similar studies can be extended to other types of welds of different shapes. The weld extraction is first step to any automatic weld inspection system; the next step can be more challenging integrating with the proposed method for weld extraction.

Bibliography

1. Cheng H.D., Yen-Hung Chen and Ying Sun, *A novel fuzzy entropy approach to image enhancement and thresholding* Signal Processing, 1999. 75: p. 277-301.
2. Noboyuki Otsu, *A threshold selection method from graylevel histograms* IEEE transactions on systems, man, and cybernetics, 1979, Vol. SMC-9, No. 1: p. 62-66.
3. Liao T.W. and Jiawei Ni, *An automated radiographic NDT system for weld inspection: part 1 – weld extraction* NDT&E International, 1996, Vol. 29, No. 3: p. 157-162.
4. Liao T.W. and K. Tang, *Automated extraction of welds from digitized radiographic images based on MLP neural networks* Applied artificial intelligence, 1997, 11: p. 197-218.
5. Liao T.W., D.-M. Li, Y.-M., Li, *Detection of welding flaws from radiographic images with fuzzy clustering methods* Fuzzy sets and systems, 1999, 108: p. 145-158.
6. Liao T.W., Damin Li, Yueming Li, *Extraction of welds from radiographic images using fuzzy classifiers* Information sciences, 2000, 126: p. 21-40.
7. Liao T.W., *Fuzzy reasoning based automatic inspection of radiographic welds: weld recognition* Journal of intelligent manufacturing, 2004, 15: p. 69-85.
8. Wang Xin and Brian Stephen Wong, *Radiographic image segmentation for weld inspection using a robust algorithm* Research in nondestructive evaluation, 2005, 16: p. 131-142.
9. Ihor O. Bohachevsky, Mark E. Johnson and Myron L. Stein, *Generalized simulated annealing for function optimization* Technometrics, 1986, Vol. 28, No. 3: p. 209-217.
10. Rafael C. Gonzales and Richard E. Woods, *Digital Image Processing* Addison-Wesley Publishing Company, 1993.
11. Witold Pedrycz and Fernando Gomide, *An introduction to fuzzy sets* The MIT Press, 1998.
12. Wang G. and Liao T.W., *Automatic identification of different types of welding defects in radiographic images* NDT & E International, 2002, Vol. 35, No. 8: p. 519-528.
13. M.K. Felisberto, H.S. Lopes, T.M. Centeno and L.V.A. Arruda, *An object detection and recognition system for weld bead extraction from digital radiographs* Computer vision and image understanding, 2006, 102: p. 238-249.
14. Nitin Aggarwal and William Clem Karl, *Line Detection in Images through Regularized Hough Transform* IEEE transactions on image processing, 2006, Vol. 15, No. 3

15. Shannon, C.E., and W.W. Weaver, *The mathematical theory of communication*, 1949, Urbana: University of Illinois press.
16. Koulmas C, SR Antony and R Jaen, *A survey of Simulated annealing applications to Operations Research problems* International journal of management Science, 1994, Vol. 22, No. 1: p. 41-56.
17. Daftardar, S., *Laser assisted friction stir welding: Finite volume method and meta-heuristic optimization*, MS Thesis, Louisiana State University, 2009.
18. Ghazavi, Sean Najm, *Computer-Aided weld inspection by fuzzy modeling with selected features*, MS Thesis, Louisiana State University, 2007.
19. Cheng H.D. and Jim-Rong Chen, *Automatically determine the membership function based on the maximum entropy principle* Information Sciences, 1997, 96: p. 163-182.
20. Witold Pedrycz, *Fuzzy equalization in the construction of fuzzy sets* Fuzzy sets and systems, 2001, 119: p. 329-335.
21. Rafael C. Gonzales, Richard E. Woods and Steven L. Eddins, *Digital Image processing using Matlab* Prentice Hall, 2004.
22. Amin Sarafray, *Line Detection via Standard Hough Transform*, Mathworks Inc. Matlab Central File Exchange, 2004. <<http://www.mathworks.com/matlabcentral/>>
23. Alina Monica Trifas, *Medical Image Enhancement* Dissertation, Louisiana State University, 2005.
24. Nikhil R. Pal and Sankar K. Pal, *A Review on Image Segmentation techniques* Pattern Recognition, 1993, Vol. 26, No. 9: p. 1277-1294.
25. L. A. Zadeh, *Fuzzy sets* Information and control, 1965, 8: p. 338-353.
26. MATLAB, *Image processing toolbox 7-User's guide* Mathworks Inc., Massachusetts, 2009.
27. T Y Lim, M M Ratnam and M A Khalid, *Automatic weld bead extraction from digitized radiographs using gray level intensity profiles and least-squares fitting* Insight, 2008, Vol. 50, No. 1: p. 8-13.
28. Y. H. Ou and Y. L. Song, *Weld location extraction in radiographic images using fuzzy rules generating method* Science and Technology of welding and joining, 2007, Vol. 12, No. 1: p.63-66.
29. Liao T.W., Aivars K. Clemins, Robert J. Hammell II, *A fuzzy c-means variant for the generation of fuzzy sets* Fuzzy sets and systems, 2003, 135: p. 241-257.

30. Hafizal Yazid, Haniza Yazid, Mohd Harun, Shukri Mohd, A. Aziz Mohamed, Mohamed Rizon, Shahrudin Sayuti, *Circular discontinuities detection in welded joints using Circular Hough Transform* NDT&E International, 2007, 40: p. 594-601.
31. Liao T.W. and Yueming Li, *An automated radiographic NDT system for weld inspection: Part II-Flaw Detection* NDT&E International, 1998, Vol. 31, No.3: p. 183-192.
32. Mehmet Sezgin and Bulent Sankur, *Survey over image thresholding techniques and quantitative performance evaluation* Journal of electronic imaging, 2004, 13: p. 146-165.
33. John D'Errico, Surface fitting using gridfit, Mathworks Inc. Matlab Central File Exchange, 2005. <<http://www.mathworks.com/matlabcentral/>>

Vita

Rakesh Gunaseelan was born in Thanjavur, an agricultural town in the state of Tamilnadu in India. He received his Bachelor of Technology degree in Industrial Engineering from Dr. B R Ambedkar National Institute of Technology, India on May 2005. Upon graduation, he worked as a software developer for about 2 years in Wipro Ltd. in Bangalore, India. Interested in automation, operations research, manufacturing systems and optimizing processes he chose Industrial Engineering as his major and enrolled in Louisiana State University on August 2007. He began working on metaheuristics and artificial intelligence under the supervision of Dr. T. Warren Liao. The degree of Master of Science in Industrial Engineering will be conferred at the August 2010 commencement.